REPORT DOCUMENTATION PAGE

Form Approved
OMB No. 0704-0188

1. REPORT DATE *(DD-MM-YYYY)*	**2. REPORT TYPE**	**3. DATES COVERED** *(From - To)*
05-10-2013		

4. TITLE AND SUBTITLE

Turbulent Boundary Layer Flow over Superhydrophobic Surfaces

5a. CONTRACT NUMBER

5b. GRANT NUMBER

5c. PROGRAM ELEMENT NUMBER

6. AUTHOR(S)
Rydalch, Andrew Jeffrey

5d. PROJECT NUMBER

5e. TASK NUMBER

5f. WORK UNIT NUMBER

7. PERFORMING ORGANIZATION NAME(S) AND ADDRESS(ES)

8. PERFORMING ORGANIZATION REPORT NUMBER

9. SPONSORING / MONITORING AGENCY NAME(S) AND ADDRESS(ES)
U.S. Naval Academy
Annapolis, MD 21402

10. SPONSOR/MONITOR'S ACRONYM(S)

11. SPONSOR/MONITOR'S REPORT NUMBER(S)
Trident Scholar Report no. 421 (2013)

12. DISTRIBUTION / AVAILABILITY STATEMENT

This document has been approved for public release; its distribution is UNLIMITED.

13. SUPPLEMENTARY NOTES

14. ABSTRACT

The objective of this project was to determine whether drag caused by turbulence in boundary layer flow can be reduced through the use of modified surfaces. This study encompassed the testing of four different surfaces: 1) Teflon SLIP, 2) Aluminum SLIP, 3) Honeycomb Superhydrophobic and 4) Polydimethylsiloxane elastomer (PDMSe) Superhydrophobic. Each of these surfaces uses specific geometrical surface features to modify the original water-surface interface. Due to the influence of the Green Fleet Initiative and the Navy's goal to increase the fleet efficiency, the Office of Naval Research is interested in determining the effectiveness of these surfaces in boundary layer flow under operating conditions similar to those in which Navy ships operate. The goal of this study was to provide data and analysis detailing the effect of these surfaces on boundary layer turbulence and drag reduction. The performance of each surface was compared with that of a smooth wall under similar operating conditions to characterize the effectiveness of each modified surface.

15. SUBJECT TERMS
superhydrophobic, SLIP, drag reduction, honeycomb

16. SECURITY CLASSIFICATION OF:			**17. LIMITATION OF ABSTRACT**	**18. NUMBER OF PAGES**	**19a. NAME OF RESPONSIBLE PERSON**
a. REPORT	**b. ABSTRACT**	**c. THIS PAGE**		49	**19b. TELEPHONE NUMBER** *(include area code)*

U.S.N.A. --- Trident Scholar project report; no. 421 (2013)

Turbulent Boundary Layer Flow over Superhydrophobic Surfaces

by

Midshipman 1/c Andrew J. Rydalch
United States Naval Academy
Annapolis, Maryland

_____

Certification of Adviser(s) Approval

Professor Ralph Volino
Mechanical Engineering Department

_____

_____

Professor Michael P. Schultz
Naval Architecture and Ocean Engineering Department

_____

_____

Acceptance for the Trident Scholar Committee

Professor Maria J. Schroeder
Associate Director of Midshipman Research

_____

_____

USNA-1531-2

1. Abstract

Drag is a force that opposes motion. This force affects objects moving through any viscous fluid, such as a plane moving through the air, a car driving down the road (through air), and a ship traveling through water. Based on an object's geometry and velocity, it experiences different forms of viscous drag as it moves through a fluid medium, characterized by the Reynolds number. In most practical applications where drag is a major factor, such as a ship sailing through the water, the Reynolds numbers are high and the flow is turbulent. The objective of this project was to determine whether drag caused by turbulence in boundary layer flow can be reduced through the use of modified surfaces. This study encompassed the testing of four different surfaces: 1) Teflon SLIP, 2) Aluminum SLIP, 3) Honeycomb Superhydrophobic and 4) Polydimethylsiloxane elastomer (PDMSe) Superhydrophobic. Each of these surfaces uses specific geometrical surface features to modify the original water-surface interface. Due to the influence of the Green Fleet Initiative and the Navy's goal to increase the fleet efficiency, the Office of Naval Research is interested in determining the effectiveness of these surfaces in boundary layer flow under operating conditions similar to those in which Navy ships operate. The goal of this study was to provide data and analysis detailing the effect of these surfaces on boundary layer turbulence and drag reduction. The testing was conducted in the small water tunnel in the USNA Hydromechanics Laboratory which operates in boundary layer flow conditions capable of producing fully developed turbulence. The effect of the surfaces on turbulence and drag reduction was measured using Laser Doppler Velocimetry (LDV). The performance of each surface was compared with that of a smooth wall under similar operating conditions to characterize the effectiveness of each modified surface.

Keywords: superhydrophobic, SLIP, drag reduction, honeycomb

2. Acknowledgements

The author would like to thank the following groups for assistance throughout the project:

- Office of Naval Research
- Harvard University
- Princeton University
- Pennsylvania State University
- University of Florida
- US Naval Academy
- USNA Trident Research Committee

3. Table of Contents

4. Introduction/Background

Motivation

As part of the Green Fleet Initiative and in response to the current economic situation, the Navy is attempting to reduce its expenditures by increasing its energy efficiency. Because viscous drag constitutes approximately half of the drag on a vessel, the Office of Naval Research (ONR) is investing heavily in viscous drag reduction research. If the Navy can reduce the amount of viscous drag a ship experiences by 10%, it will result in 5% less energy needed for its ships, which will result in 5% less fuel consumed, which will save 5% of the money spent on fuel. Currently, the average Arleigh Burke Guided Missile Destroyer requires $11.1M each year for fuel (Schultz et al. 2011). A viscous drag reduction of 10% would amount to a savings of $550k per destroyer each year. Reductions of 20% would save over one million dollars per destroyer each year. Currently, the Navy has over fifty operating Arleigh Burke Destroyers, which make up only 30% of the surface fleet. Reducing 20% of the viscous drag could save the Navy over $50M each year on the destroyer class and similar technology could be applied to the other surface ships for even greater savings. In addition to saving money for the Navy, viscous drag reduction is also highly valued in the global shipping industry where the savings would be on the order of billions of dollars annually. Because there is high potential for saving significant amounts of money, the drag reduction field has been, and will continue to be, deeply researched.

This project is of great value to the Navy and commercial industry because it provides a deeper understanding of how microfeatures affect boundary layer flow. If any of the surfaces tested effectively reduced drag in a turbulent, boundary layer flow, the next step would be to begin the process of applying this technology to ships. If the research proved that the microfeatures have no significant effect in boundary layer flow, new data will be gained that addresses why the features are ineffective and the Navy can move in a different direction. Whether the tests succeed or fail at reducing drag, the data collected in this study is of significant value.

The Physics

As a ship moves through the water, drag resists the motion. The drag experienced by the ship is divided into two basic types, “wave-making” drag and “viscous” drag. As its name implies, wave-making drag occurs as the ship pushes water out of its path, thus creating waves. As evidenced by wake patterns through water, wave-making drag is relatively low at low speeds and has increasing effect as the speed increases. The wake and the waves generated are largest

when ships approach their maximum speed. Viscous drag, however, is the dominant drag force at normal operating speeds. Viscous drag comes in two types, "frictional" drag and "form" drag (Makiharju et al. 2008). Frictional drag results from friction between the hull of the ship and the water that it is moving through: the water resists the motion of the ship. Form drag, a significantly weaker component, results from a pressure differential along the length of the ship. Along with wave-making drag, modern ship design has minimized the effects of form drag. At cruising speeds where U.S. Navy ships operate approximately 90% of the time (Schultz et al. 2011), frictional drag is the largest component of the drag force opposing the ship's motion. This project focused on research into minimizing the effect of viscous drag.

Viscous drag is often quantified as the magnitude of the shear stress at the wall. Due to both friction between the surface and the fluid and the physical properties of the fluid, a flow will develop a velocity gradient as it moves over a wall, as depicted in Figure 1.

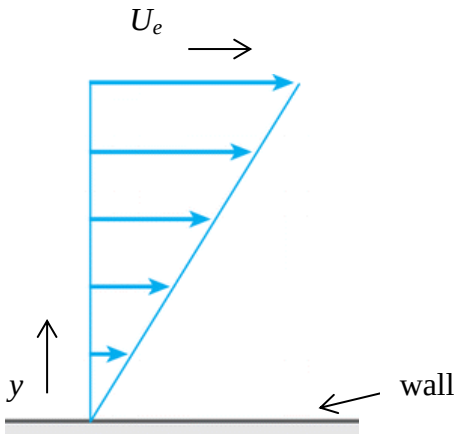

Figure 1: Velocity Gradient (adapted from Rothstein 2010)

Infinitesimally close to the wall, the fluid exhibits a "no-slip" condition where its velocity is equal to the velocity of the wall, in this case zero. As shown in the figure, the velocity of the flow (u) increases as its distance (y) from the wall increases. As this distance increases, the velocity of the fluid eventually reaches the velocity of the "free-stream," which is the velocity of the flow that is completely unaffected by friction with the wall. This portion of the flow, from the wall to the free-stream, is referred to as the "boundary layer," with its thickness being referred to as the boundary layer thickness (δ). Another important factor contributing to the boundary layer thickness, and therefore the viscous drag, is the viscosity (μ) of the fluid. For example, if the fluid in Figure 1 were a highly viscous fluid, such as honey, the boundary layer would be thick while if the fluid were water, a low-viscosity fluid, the boundary layer would be much thinner. Essentially, viscosity is a measurement of a fluid's resistance to shear. A fluid with a higher viscosity will experience more shear stress, and thus more drag, than a fluid of a lower viscosity at the same shear rate. Shear stress (τ) is the force per unit area and is defined as:

$$\tau = \mu \frac{du}{dy} \qquad (1)$$

In addition to determining the amount of viscous drag, the velocity and viscosity of a fluid also determine the characteristics of the flow. When the relative velocity between a surface

and a fluid is small, the flow is typically categorized as “laminar.” As the name implies, a laminar flow exhibits smooth, even flow throughout the boundary layer. This results in low drag, because the fluid is able to smoothly move over the surface. When the relative velocity is large, the resulting flow is defined as turbulent and is characterized by disturbances such as eddies and other flow instabilities. The turbulent condition results in fluid moving at non-uniform velocities closer to the wall of the object, which creates a larger velocity gradient that increases the shear stress and results in more drag. Figure 2 shows the differences between laminar and turbulent conditions.

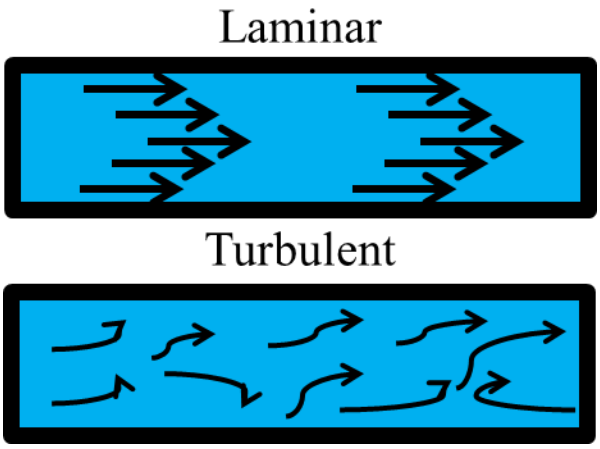

Figure 2: Laminar and Turbulent Flows

The transition from laminar to turbulent flow depends on the ratio of the inertia of the fluid to the viscous force resisting motion. A higher inertia in the fluid increases perturbations in the fluid’s velocity and tends to produce a more turbulent flow. Inversely, greater viscosity results in larger viscous forces that can damp out the perturbations caused by the inertia, producing a more laminar flow. This non-dimensional ratio is defined as the Reynolds number

$$Re = \frac{\rho u L}{\mu} \qquad (2)$$

where ρ = fluid density and the inertial forces are proportional to $\rho u^2 L^2$ which represents the product of the fluid’s density with the square of the characteristic velocity and characteristic length. The viscous force is proportional to $\mu u L$. The ratio of the inertial and viscous forces results in Equation (2). At low Reynolds numbers, the flow is typically laminar while higher Reynolds numbers result in more turbulent flows. In most practical engineering applications Reynolds numbers are high and the flow is turbulent. In this project, the friction Reynolds number (Re_τ), also referred to as the Kármán number, will be used to characterize the flow. The friction Reynolds number is as defined in Equation (2), but with a particular characteristic length and velocity. The characteristic length for a channel flow is half the channel height, and for a boundary layer flow the characteristic length is the thickness of the boundary layer, δ. The characteristic velocity for both types of flows is the friction velocity, u_τ, which is defined as the square root of the shear stress at the wall, τ_w, divided by the fluid density (ρ), as shown in Equation (3).

$$u_\tau = \sqrt{\frac{\tau_w}{\rho}} \qquad (3)$$

The objective of this project is to determine whether it is possible to create slip in the "no-slip" zone at the boundary between the object and the fluid, depicted in Figure 3. If slip can be generated, the velocity of the fluid at the surface will no longer be zero, thus resulting in a weaker velocity gradient, lower shear stress, and less drag. A smaller boundary layer results in a lower effective Reynolds number which could possibly result in lower levels of turbulence or perhaps even laminar flow which would further reduce the drag.

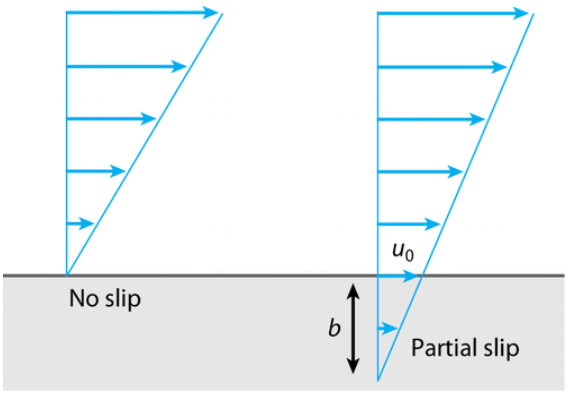

Figure 3: Slip at the Wall (Rothstein 2010)

Relevant Studies

Throughout history, efforts have been made to reduce the effect of drag. Effectively reducing form and wave-making drag, ship design has evolved the V shape and water-breaking prow. Since the advent of automobiles, airplanes, and modern ships, effectively reducing viscous drag has become even more important. In response to this need, and with the benefit of modern technology, the drag-reduction field is replete with attempts to accomplish this goal. Essentially, the different methods at reducing drag can be divided into three different approaches: 1) modifications of the physical surface to reduce turbulence in the flow, 2) modifications of the fluid properties to reduce turbulence, and 3) modifications of the fluid-surface interface to reduce turbulence.

Surface Modifications

In 1937, Kramer, a German scientist, patented a new idea of running thin wires over the edge of a surface in order to modify the flow (Hefner 1990). Today, Kramer's idea has evolved and some modern ships and planes are manufactured with "riblets," small ridges on the order of fractions of millimeters, built-into the hull or skin that seek to reduce frictional drag. The riblets run in the streamwise direction of the flow and reduce the spanwise turbulence. By reducing the effects of the cross flow, turbulence and drag are reduced along the surface. According to recent data (García-Mayoral and Jiménez 2011) these riblets can result in up to a 10% reduction in drag experienced at the vessel's surface. In spite of the potential shown in experiments, difficulties in

the manufacture and maintenance of riblets have decreased their practical effectiveness, and researchers are still searching for a more effective method at reducing drag.

Fluid Modifications

One of the most effective drag reduction techniques in practice today comes from the use of polymer additives. Polymers added to the flow act as a force that dampens the magnitude of the turbulence, and thus reduces drag. This technology has proven effective in channel flow conditions, and is currently used in oil pipelines. The drag-reducing effect that long-chain polymer additives have over a surface was discovered as early as 1946 (Toonder 1995). Lumley (1973) detailed the attempts of researchers to modify the flow characteristics by introducing trace percentages of specific polymers to the flow. Recently, this field has expanded to include not only the effectiveness of specific polymers, but the effectiveness of their shape as well (Amarouchene et al. 2008). Unfortunately, additive polymers are not feasible options for ships, due to the impracticality of continuously polluting the water with inorganic materials, but the concept of modifying the fluid itself to reduce drag is relevant.

Building upon this concept, studies have been conducted on the introduction of environmentally friendly air bubbles, rather than polymers, into the flow. At the United States Naval Academy, McCormick and Bhattacharyya (1973) used electrolysis to generate microbubbles at the edge of a submerged surface. These microbubbles reduced the amount of viscous drag on the order of 5% (Kodoma et al. 2000); however, the technology has not been practically applied on ships due to further questions regarding the exact mechanism of the drag reduction and the increased energy required to generate the bubbles.

Fluid-Surface Interface Modifications

Recently, rather than modifying either the surface or the fluid individually, research has been conducted on the practicality of modifying the fluid-surface interface itself. Figure 4 shows the theory behind Air Layer Drag Reduction (ALDR) which attempts to replace the fluid-surface interface with a fluid-fluid interface. This technology uses air jets to insert a complete layer of air between a surface and the fluid. Ideally, this concept reduces all of the drag, and reductions on the order of 100% have been reported in the laboratory (Elbing et al. 2008); however, Elbing et al. (2008) also report that these reductions were only seen in immediate proximity to the air jet inserting the air. As the distance from the jet increases, the drag increases drastically. Also, researchers have had difficulty in maintaining a stable air-fluid interface over time. Similar to generating microbubbles, the requirement of using energy to insert the air in the system has stopped this concept from being developed practically.

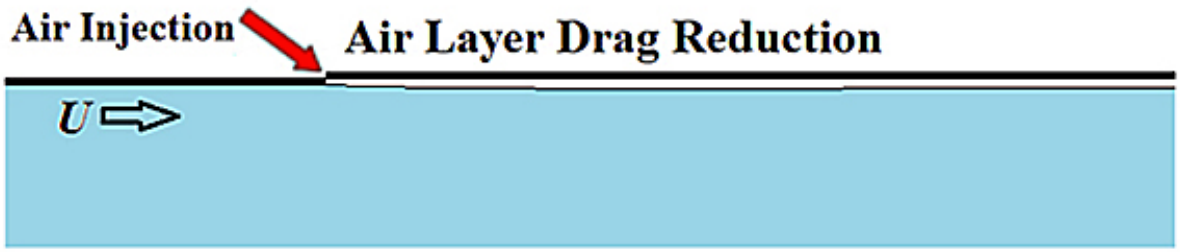

Figure 4: Air Layer Drag Reduction (Perlin and Ceccio 2013)

In an attempt to create a stable air-fluid interface, the Superhydrophobic Surface (SHS) has been developed. As shown in Figure 5, these surfaces are designed in such a way that the flow moving over the wall interacts with both air and the wall, rather than only with the wall as in a traditional case or only with the air as in ALDR. Superhydrophobic surfaces are hydrophobic surfaces, meaning they repel water, that contain surface microfeatures on the order of tens of micrometers which alter the fluid-surface interface. These features range from "mountain-valley" motifs, shown in Figure 5, to "posts" that dot the surface. Due to surface tension properties, water is unable to permeate the minute grooves created by the microfeatures and results in an air-fluid interface that decreases the contact surface area of the fluid-surface interface and significantly reduces the drag, on the order of 50% (Martell et al. 2009; Daniello et al. 2009). Superhydrophobicity is both a factor of the geometry of a surface and the wettability of the material. Pioneering work in this field was carried out by the research group of Professor J. Rothstein at the University of Massachusetts and is described in the recent papers of Martell et al. (2010) and Muralidhar et al. (2011). Researchers hypothesize that SHSs can have a significant effect on drag experienced by marine vessels; however, several questions remain regarding the application of these surfaces to drag reduction for marine vehicles.

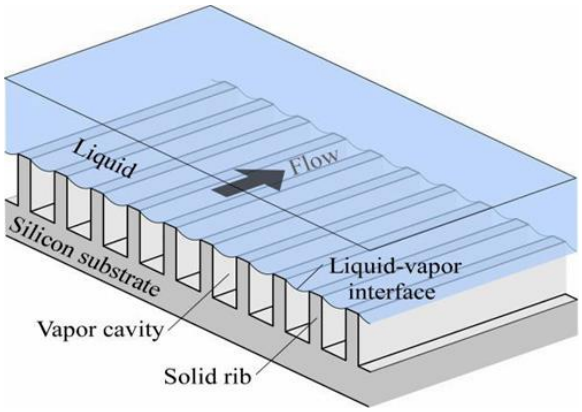

Figure 5: Superhydrophobic Surface (BYU 2013)

Although pioneering work has been conducted on SHSs, their performance in turbulent, boundary layer flow is undetermined. Rothstein's successful experiments were conducted in an internal, channel flow environment. In a channel, the fluid is bounded by solid surfaces on all sides, as depicted in the water velocity diagram in Figure 6. The velocities vary from zero at the walls to a maximum velocity towards the center of the channel. There is no "freestream" in this type of flow. Rothstein's experiments indicated that the microridges are effective at reducing drag in the channel flow conditions tested, but marine vessels do not operate in these conditions.

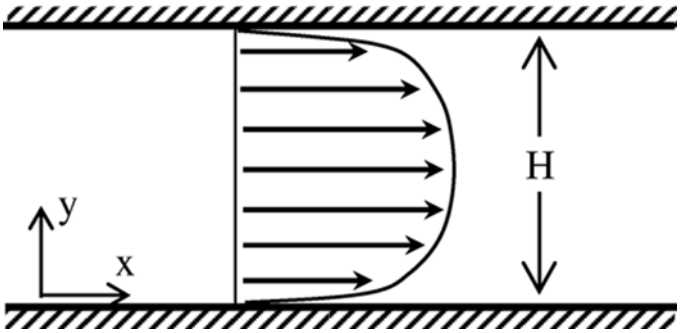

Figure 6: Internal Flow through a Pipe (Esmail 2005)

The flow of the water in a boundary layer flow is only constrained on one side. As depicted in Figure 7, the flow is only disrupted by the wall on the bottom edge. The relative velocity is zero at the wall and increases until it reaches the free-stream velocity (U_e). At this distance from the wall, the velocity of the water is not affected by the surface. This differs from channel flow where the entire flow field is influenced by the surface. As a result, the flow characteristics and drag magnitude in a boundary layer differ from those in channel flow. Due to these fundamental differences, it is not clear that a superhydrophobic surface will yield drag reduction in a boundary layer flow.

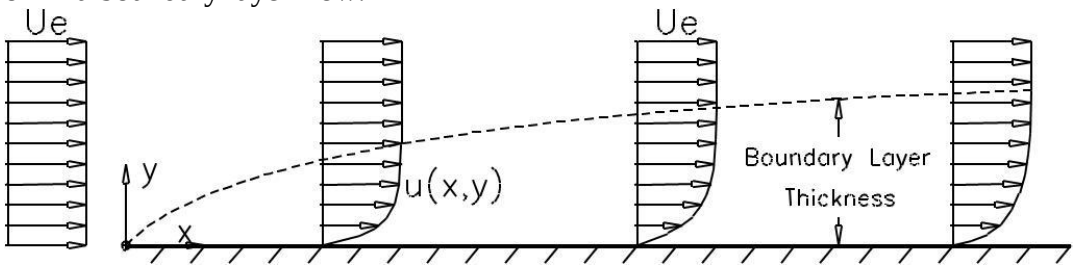

Figure 7: Boundary Layer Flow (Schultz, 2011)

Another unanswered question regarding superhydrophobic surfaces is the fundamental mechanism that gives rise to the observed drag reduction. Rothstein hypothesized that the drag reduction was caused by the microfeatures trapping air on the surface. This was based on the visual observation of Daniello et al. (2009) who pointed out the surface's "silvery appearance" when it was fully immersed in water. While this supports Rothstein's hypothesis, it is possible that the microfeatures are reducing drag through some other mechanism. Currently, there has been no direct confirmation that the microfeatures allow slip and reduce drag through the establishment of an air-water interface.

Finally, it is unresolved as to whether drag reduction using superhydrophobic surfaces is feasible at high Reynolds numbers. The experiments of Rothstein were conducted in turbulent flow conditions; however, the Reynolds numbers were quite small. For example, the largest friction Reynolds number tested was on the order of 600 (Daniello et al. 2009). It is not altogether clear if the drag reduction observed at low friction Reynolds numbers will extend to the higher friction Reynolds numbers that typify the normal operating conditions of most marine vessels. Ships generally experience friction Reynolds numbers over 10,000.

The Test Surfaces

Slippery Liquid Infused Porous Surface (SLIP Surface)

Based on the idea of modifying the fluid-wall interaction, SLIP surfaces have been developed by Dr. Aizenburg of Harvard University. The SLIP surface traces its origins to nature and the *Nepenthes* pitcher plants. The walls of these plants are completely saturated with a syrupy fluid that captures insects. The idea of the SLIP surface, as contained in the name, is to saturate a porous material, referred to as the "substrate," with low viscosity oil, the "lubricant", to the extent that a thin film of lubricant covers the entire surface. Theoretically, the fluid passing over the SLIP surface will interact with the lubricant rather than the substrate itself, and result in slip along the substrate. Figure 8 illustrates this idea.

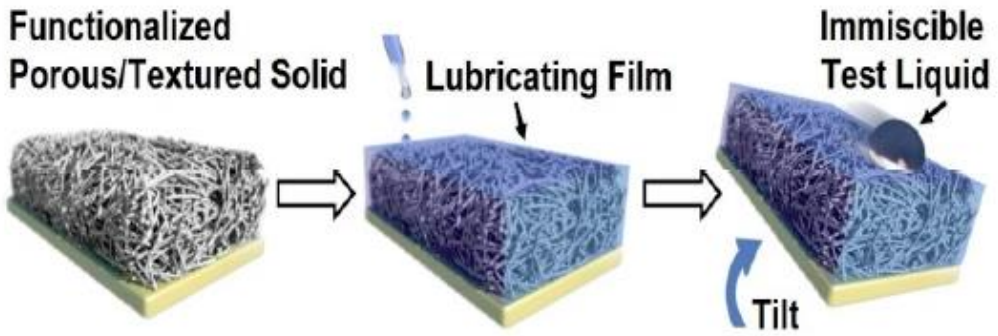

Figure 8: SLIP Surface Principles (courtesy of Dr. Aizenberg)

The SLIP surface concept is just reaching the experimental stage. Several of these surfaces have been produced by Dr. Aizenburg and distributed to researcher groups at Princeton University and the United States Naval Academy. The objective of the researchers is to determine the effectiveness of these surfaces in reducing drag. Because these surfaces have just been developed, these materials have never been experimentally tested and there is currently no existing data to document their performance. Two different substrate surfaces were obtained for testing as a part of this project. The objective was to determine the effectiveness of the SLIP surface in reducing drag in a turbulent boundary layer flow. In agreement with the purpose of the other research groups, the effect of the different substrates and lubricants on the turbulent flow was documented.

Substrates

The first SLIP surface tested used a Teflon substrate and is shown in Figure 9. This substrate was selected in an attempt to capitalize on the inherent hydrophobicity of the Teflon material. The Teflon surface has an inherent affinity for the Teflon oil which was used as the lubricant. The Teflon surface was ~30 cm in length and was fixed to an acrylic sheet. The testing piece was obtained from the research group at Princeton University.

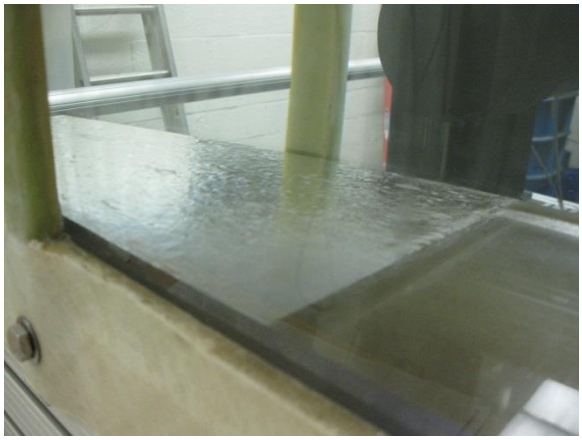

Figure 9: Teflon 100 surface

The second SLIP surface tested used an aluminum substrate. Aluminum was chosen in order to test the effectiveness of the SLIP concept on metals. The substrate was created using a unique manufacturing procedure developed at Harvard University. The process begins with a sheet of stock aluminum of the desired size for testing. The aluminum is sanded down with 600 grit sandpaper in preparation for the surface treatments. Once prepared, the aluminum sheets are "boehmitized," subjected to processes that modify both physical and chemical properties of the surfaces. In the boehmetizing process, the test section is soaked in boiling water for approximately ten minutes. This allows for the growth of a surface nanostructure, on the scale of 10-30 nanometers. Figure 10 is the scanning electron microscope image of the nanostructure. Upon being boehmitized, the surfaces are then "functionalized" by a chemical reaction that links the substrate to the lubricant. This is done by soaking the boehmitized aluminum in a "fluorination bath." The fluorination process can be controlled in such a way that links the substrate to a particular lubricant. In order to fully document the performance of the aluminum substrate SLIP surface, three different test cases were conducted, each different from the other based on the type of lubricating oil. Initially, three 8 x 12 in. sheets of 1/8 in. thick aluminum stock were cut and sanded down with 600 grit sandpaper in the USNA workshop. These pieces were sent to the facilities at Princeton University for boehmitization.

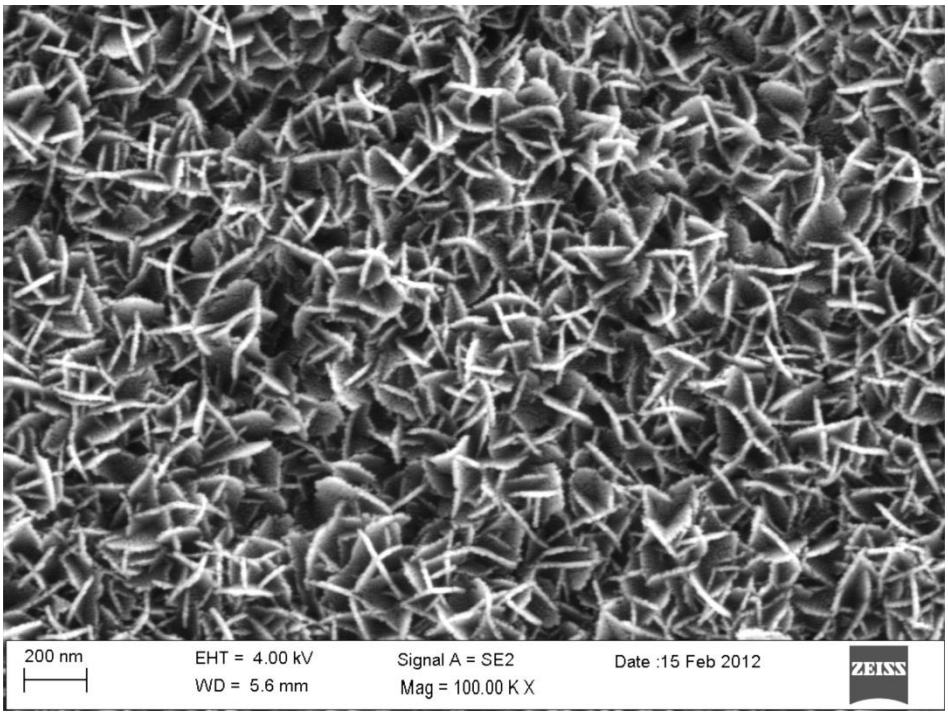

Figure 10: Scanning Electron Microscope image of the boehmite (Kim 2013)

Lubricant

Two different lubricants were used throughout the testing of the SLIP surfaces. These lubricants and their respective kinematic viscosities in centi-Stokes (cSt) are shown and compared with the kinematic viscosity of water in Table 1. Although the Krytox oils are more viscous than water, they are theoretically expected to reduce drag because their viscosity is far less than that of a solid surface. Interestingly, preliminary studies conducted by the Princeton research group indicate that the Krytox 102 oil may be more effective than the lower viscosity Krytox 100 oil at reducing drag over time. This project determined which of the lubricants is more effective under turbulent, boundary layer flow conditions.

Table 1: Lubricant Viscosities

Lubricant	**Viscosity (cSt at 20 C)**
Water	1
Krytox 100	12.4
Krytox 102	38

SLIP Surface Test Cases

Teflon Test Case (Teflon 100a and Teflon 100b): Teflon substrate, Krytox 100 oil.

The Teflon material, as a completely functionalized SLIP surface, was completely saturated with the Krytox 100 oil. This combination was chosen based on the inherent hydrophobicity of the Teflon material and the low viscosity of the Krytox 100 oil. In Teflon 100a, the surface was saturated with the Krytox 100 series oil once and then the entire battery of tests was run. For Teflon 100b, the surface was saturated approximately twenty-four hours before each test.

Aluminum Test Case I (Al 100): Aluminum substrate, Krytox 100 oil.

The boehmitized aluminum was functionalized to link with the Krytox 100 oil, the same oil used in the Teflon test case. The objective of this test case was to compare the performance of the aluminum and Teflon substrates, with all other conditions remaining the same.

Aluminum Test Case II (Al 102): Aluminum substrate, Krytox 102 oil.

The boehmitized aluminum was functionalized to link with the Krytox 102 oil. The objective of this test case was to determine whether using a more viscous lubricant would result in reduced skin friction over time.

Aluminum Test Case III (Al no oil): Boehmitized aluminum substrate, no lubricating oil.

The processing of this surface stopped after the aluminum was boehmitized; the nanostructure was never saturated with oil. The objective of this case was to determine the effectiveness of the boehmitized substrate as a superhydrophobic surface. Due to the surface tension properties of water, it is possible that the functionalized boehmite nanostructure could remain saturated with air when submerged in the water tunnel. Essentially, the lubricant would be air which would significantly reduce the skin friction. Technically, the aluminum in this test case is not considered a SLIP surface because it was never saturated with lubricating oil.

Honeycomb Surface

Similar to the ALDR concept, this project includes the use of honeycomb surfaces in an attempt to modify the fluid-wall interface with air. The idea is that if the cells in the honeycomb, shown in Figure 11, can be filled with air, the fluid flowing along the surface will move along the air instead of a solid surface. This will decrease the shear stress in the flow, and thus lower drag. Theoretically, the honeycomb pockets will provide a stable base upon which the air layer can develop, thus increasing the effectiveness of the drag reduction over time. The question is whether the air pockets will be able to overpower the negative effects that come from the uneven honeycomb surface. Without air in the pores, the honeycomb is a rough surface, and the drag in the flow over a rough surface is significantly greater than the drag over a smooth surface. However, there are no published results on the effects of air-filled honeycomb in a boundary layer flow. The results obtained in this project are the first of their kind. The cell size selected for this investigation was 3 mm.

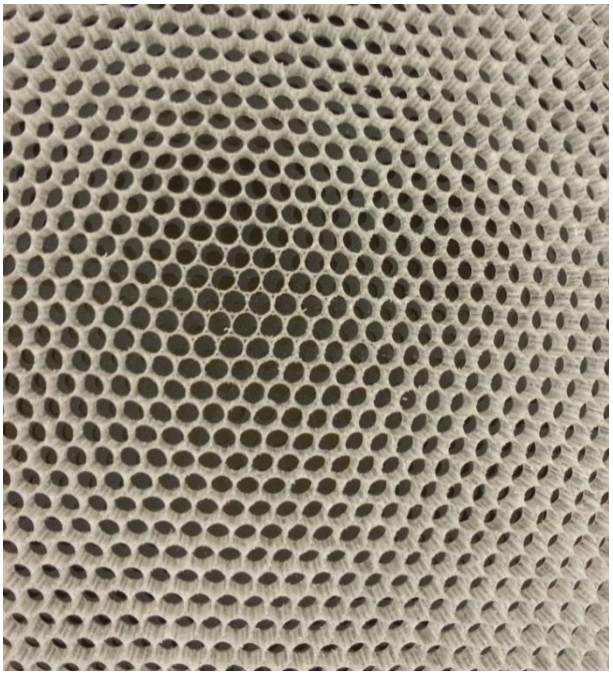

Figure 11: Honeycomb Surface

Superhydrophobic Surface (SHS)

The SHS tested in the experiment is shown in Figure 12. The entire SHS is ~15 cm and is made from polydimethylsiloxane elastomer (PDMSe). The surface used for testing was the Silastic T-2 product, commercially available through Dow Corning. This surface was produced by Professor Tony Brennan from the University of Florida. The microfeatures on this surface are arranged in the mountain and valley motif, shown previously in Figure 5. The ridges are on the order of 50 μm in depth, running from the left to the right. This surface was fixed to a smooth acrylic wall on the bottom of the water tunnel for testing.

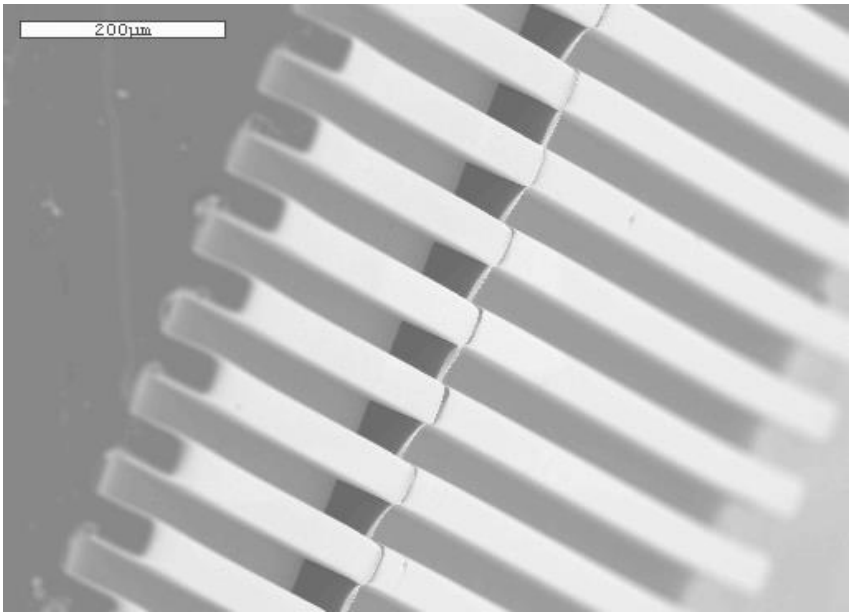

Figure 12: SEM of the Superhydophobic Surface

5. Experimental Details and Theoretical Analysis

The testing was conducted in the water tunnel, pictured in Figure 13, in the Naval Academy's Hydromechanics Laboratory. In its current configuration, the water tunnel can produce the flow required to characterize of the effectiveness of a surface at reducing drag. The water tunnel is designed to produce well-controlled, boundary layer flow. This is accomplished by controlling the height of the top wall of the water tunnel.

Figure 13: USNA Hydromechanics Lab Water Tunnel

As shown in Figure 13, the top wall of the water tunnel is fitted with knobs used to adjust its height. This feature is used to ensure that free stream flow has a constant velocity throughout the testing section. This condition is referred to as zero pressure gradient flow. The test surface is affixed to the bottom wall. Water from the holding tank is pumped into the tunnel at a specific speed, determined by the user via variable-frequency drive units that control the pumps. The water tunnel is able to produce friction Reynolds numbers up to 4000 and was entirely capable of producing the conditions needed for the desired tests.

The data from the tests was collected primarily using Laser Doppler Velocimetry (LDV) technology, pictured in Figure 14.

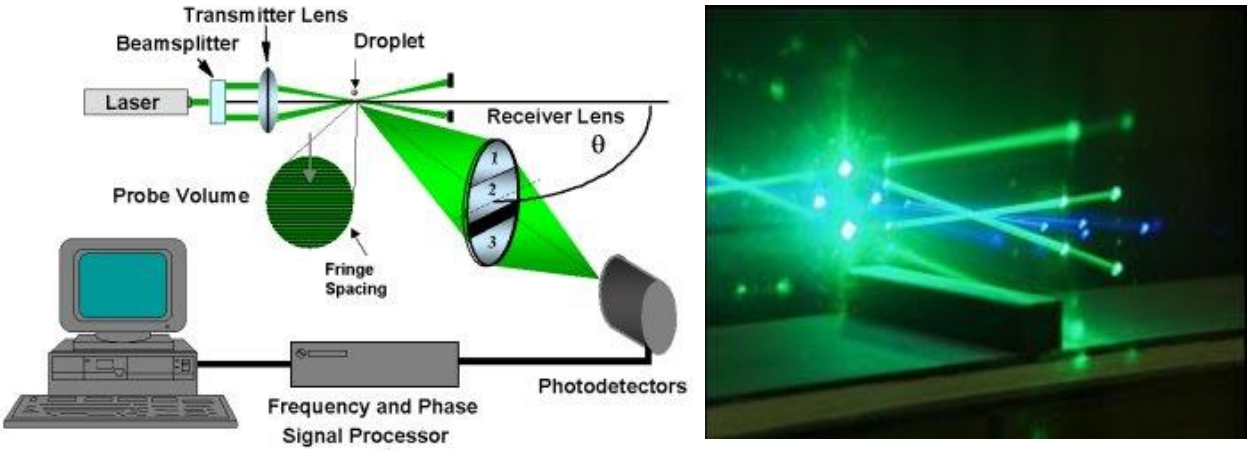

(a) (b)

Figure 14: (a) LDV process, (LaVision 2012); (b) LDV Working Photo, (RWTH 2012)

As depicted in Figure 14a, LDV focuses a laser on a specific point. The LDV in the USNA Hydromechanics lab is equipped with a multi-line laser capable of splitting into four beams, as shown in Figure 14b. The point where the beams focus is controlled by the user. In this project, the beams were focused at points along a line normal to the superhydrophobic surface. The water in the tunnel was seeded with silver-coated glass spheres 2 μm in diameter that reflected the laser light as they passed through the point of interest. The reflected laser beams were received by photodetectors and the Doppler shift was determined by a computer to yield the velocity of the flow. Essentially, the computer solves for the flow velocity *U* of the individual glass spheres to profile the water flow.

In order to fully characterize the velocity profile over the wall, the LDV was set up to collect data at specific points orthogonal to the wall. Based on the fundamental properties of boundary layer flow described by Schetz (1993), a logarithmic distribution was chosen. The distance between each data point was determined based on the operating speed of the water tunnel. A small fluid velocity results in a large boundary layer and thus requires further spaced data points while a high fluid velocity results in a smaller boundary layer with a tighter data point distribution. At $Re_\tau \sim 500$, the logarithmic distribution was based over a boundary layer of $\delta = 48.5$ mm. At $Re_\tau > 500$, the flow was measured over a nearly constant boundary layer of $\delta = 42.5$ mm.

At each data point, thousands of readings were collected. The measured velocity is actually the average of these readings. The exact number of measurements taken at each point varied with both the operating Re_τ, the higher velocity flow allowed more seed particles to pass through the LDV focus point, and the distance of the test point normal to the wall, the actual velocity of the fluid increases as the distance from the wall increases and thus more measurements could be taken. The total number of measurements at a specific point ranged from ~1000 close to the wall to ~50000 near the free stream. This range of measurements is typical of LDV measuring techniques and is accepted in the field.

Smooth Wall Tests

The first step in the project was to establish baseline values to both validate the results and set a standard to which future measurements could be compared. This was accomplished by inserting a "smooth wall" into the water tunnel, shown in Figure 15. The smooth wall is the dark colored surface shown in the figure. The height of the upper surface in the tunnel was adjusted in order to create a constant velocity, zero-pressure gradient, throughout the tunnel. Data were collected using the LDV system described above. Four different cases were run, each case having a different Re_τ. The tunnel conditions for the smooth wall tests are shown in Table 2. Data were collected at 42 points distributed logarithmically through the boundary layer of the flow. The results are discussed in Section 6 of this paper.

Table 2: Baseline Test Matrix

	U_e (m/s)	Re_τ
Run 1	0.31	500
Run 2	0.78	1100
Run 3	1.25	1500
Run 4	2.25	2500

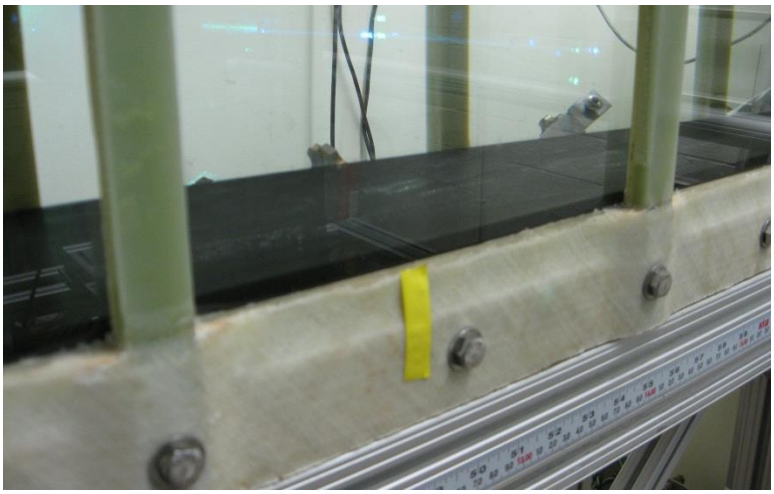

Figure 15: Smooth Wall Test

Teflon SLIP Surface Tests

The Teflon 100 surface was tested in a manner similar to the smooth surface. A new bottom wall to the tunnel was constructed by the USNA workshop. This wall was a 2.0 x 0.2 m acrylic board with a 0.28 m long, 2.5 mm deep cavity hollowed out at a distance of 1.2 m from the upstream edge of the wall, shown in Figure 16. The Teflon 100 surface was fixed in this cavity, flush with the surface of the wall, and installed into the water tunnel. Data were collected using the LDV at 42 points distributed logarithmically through the boundary layer. Four different cases were run, each case having a different Re_τ, see Table 3. The results from these first tests of the Teflon 100 surface, the "normally-oiled" test case, are referred to as Teflon 100a and are discussed in Section 6 of this paper.

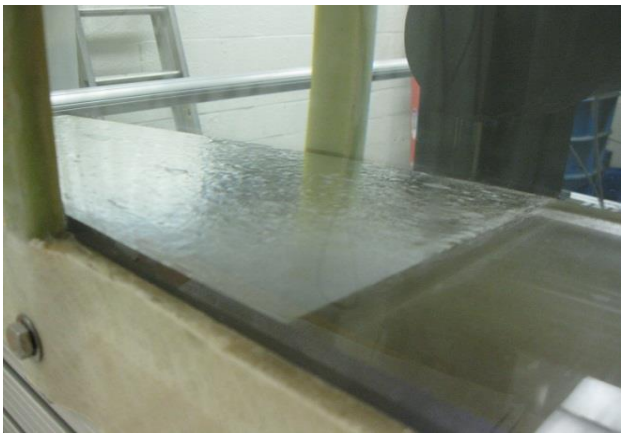

Figure 16: Teflon SLIP Surface

Table 3: Teflon 100a Test Matrix

	U_e (m/s)	Re_τ
Run 1	0.38	500
Run 2	0.78	1200
Run 3	1.25	1600
Run 4	2.25	2700

The testing plan was modified at this point due to observations of the Teflon 100a case. Visual observation showed that the oil embedded in the Teflon 100 surface was either not being fully absorbed into the SLIP material or that it was being pulled out by the rushing water. Figure 16 shows the SLIP surface before the initial testing. The hydrophobic oil is evident in the sheen over the material. The sheen was not as strong following the testing. This led to a modification in the experimental procedure and another series of testing. This testing matrix is referred to as Teflon 100b. Before each run in Teflon 100b, additional Krytox oil was applied to the SLIP material. The oil was administered using a spray bottle until the surface visually appeared saturated. The oil was allowed approximately 24 hours to soak in before running the tests. Figure 18 shows the surface as the tunnel is being filled after the 24 hour wait period. The hydrophobicity of the material is visible upon examining the height of the water in the image. Over a smooth, non-hydrophobic surface the height of the water would be much less than that shown in Figure 17. However, in order to overcome the effects of surface tension, the water is pooling up. Shortly after the image was taken, enough water had collected to overcome the surface tension and flow over the hydrophobic material. Teflon 100b was tested in the same fashion as Teflon 100a, see Table 4. The results for the second battery of testing, the “pre-oil” test case, are discussed in Section 6 of this paper.

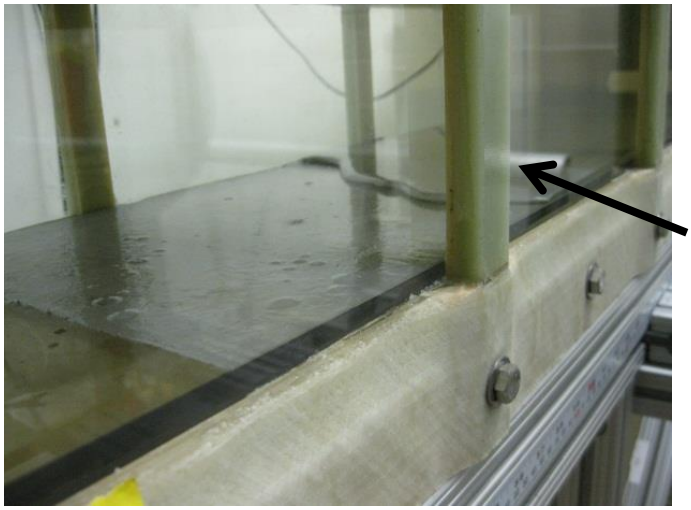

Figure 17: SLIP Surface after oil application

Table 4: Teflon 100b Test Matrix

	U_e (m/s)	Re_τ
Run 1	0.38	500
Run 2	0.78	1200
Run 3	1.25	1700
Run 4	2.25	3000

Aluminum SLIP Surface Tests

Due to the performance of the Teflon 100a and 100b SLIP Surface tests, collaboration with the research groups at Princeton and Harvard, and time constraints, the testing matrix of the Aluminum SLIP surfaces differed from the Teflon tests. Rather than testing at Re_τ ranging from low turbulence to fully developed turbulence, the Al SLIP surfaces were tested at middle levels of turbulence. The results obtained at these levels indicate the performance of the surfaces at the higher and lower Re_τ. The Al 100, Al 102, and Al no oil surfaces all followed the same test matrix, shown in Table 5.

Table 5: Al SLIP Test Matrix

	U_e (m/s)	Re_τ
Run 1	0.78	1170
Run 2	1.25	1500

Prior to testing, the Al SLIP surface was prepared by infusing the Krytox oil. As shown in Figure 18, a row of oil was applied down one edge of the surface. The surface was then rotated 90 degrees to a vertical position to allow the oil to run down the surface, Figure 19. This process was repeated until the entire SLIP surface visibly appeared to be coated in the oil, Figure 20. Upon being completely covered, the surface sat unperturbed for twenty minutes to allow the oil to completely saturate the SLIP surface.

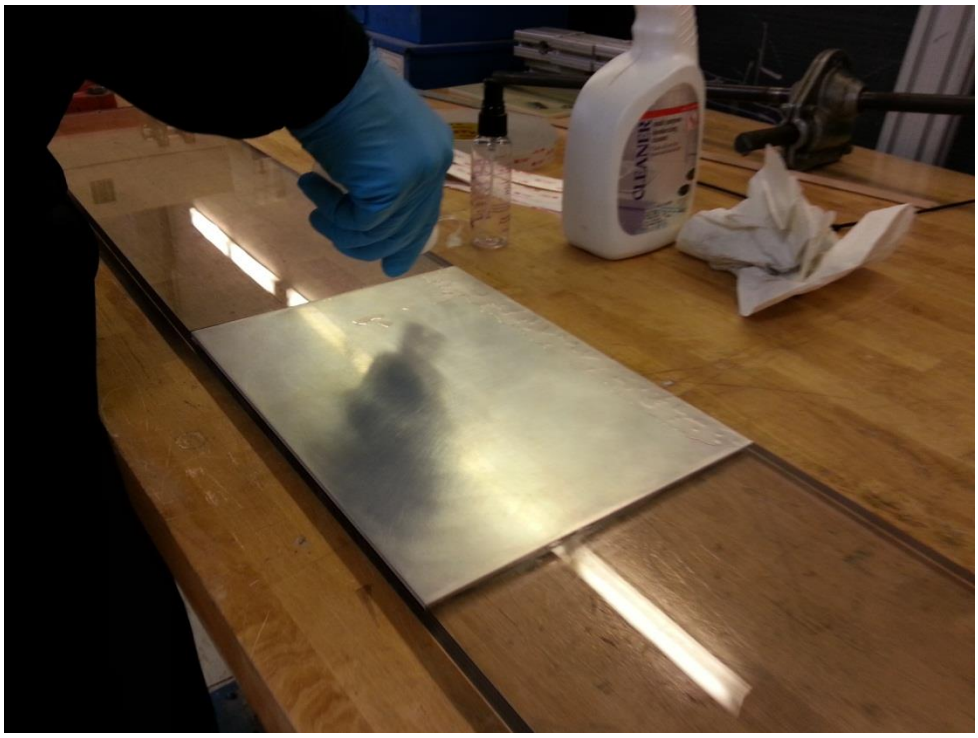

Figure 18: Applying the oil

Figure 19: Coating the Surface

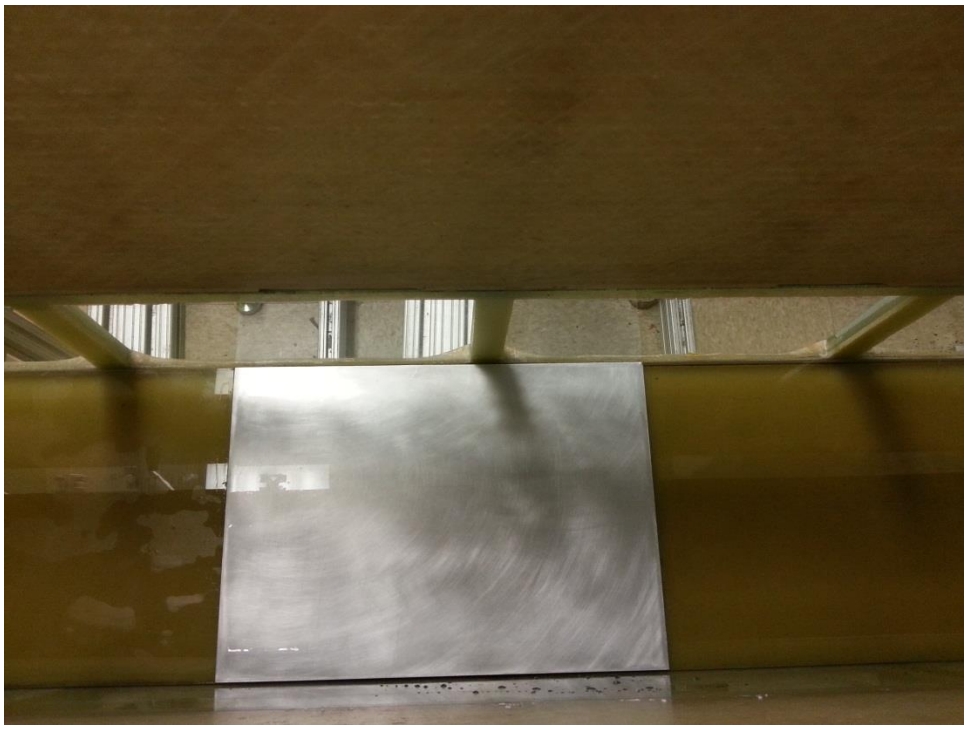

Figure 20: Completed Coating

Figure 21 shows the SLIP Surface initially after water has run over it in the water tunnel. The bright sheen is evidence that the surface remained saturated with oil. However, visual observation determined that too much oil had been applied to the surface. This was easily fixed by allowing the water to shear off the excess oil. Figure 22 shows the surface after it has been running in the water tunnel for approximately thirty minutes. It is evident that excess oil had begun migrating downstream on the surface. Figure 23 shows the surface after it has been in the water tunnel for approximately three hours. At this point, it was determined through visual observation that the saturated surface had reached a state of equilibrium. Although it is evident from the brighter sheen on the trailing edge that the oil had amassed at the end of the surface, this would not affect measurements on the upstream portion of the surface. A homogeneous testing area had developed over which accurate measurements could be obtained, marked by the red star in Figure 23.

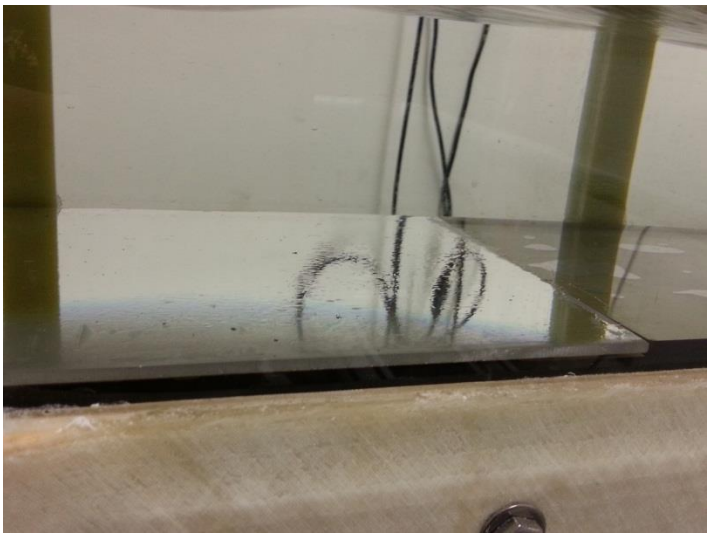

Figure 21: Initial Infusion in the Tunnel

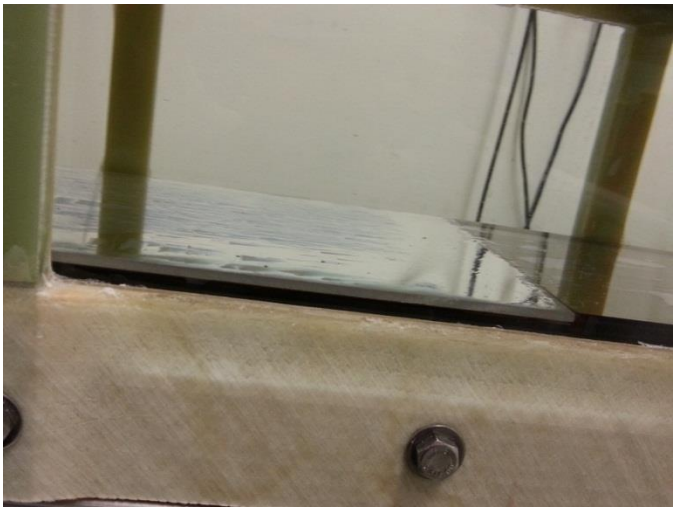

Figure 22: Surface after approx. 30 Minutes

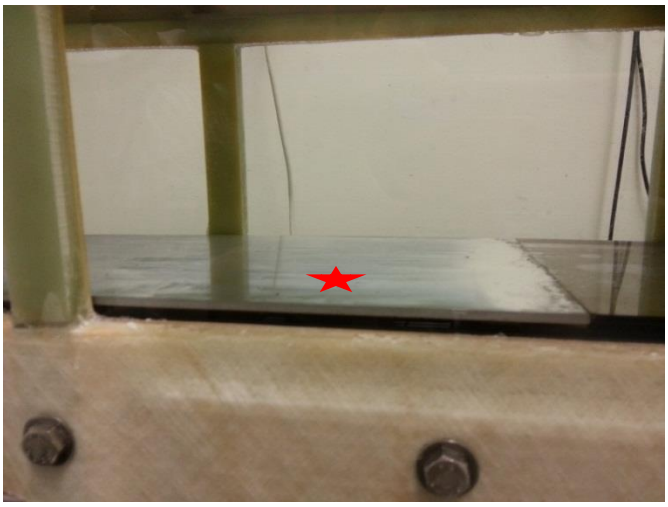

Figure 23: Surface after approx. 3 Hours

Honeycomb Tests

Initial work on the honeycomb was done in an open water tunnel, no roof attached, through visual observation of the water moving across the honeycomb. As expected, the air in the honeycomb pores was lost due to the pressure differential as the water rushed across the surface. Once filled with water, the honeycomb had no means of replenishing the air pulled out by the water flow. Because the objective of the test was to determine the effectiveness of the air pockets in the honeycomb at reducing drag, a system was designed and constructed that would replenish the air in the pockets. This system is shown in Figures 24 and 25.

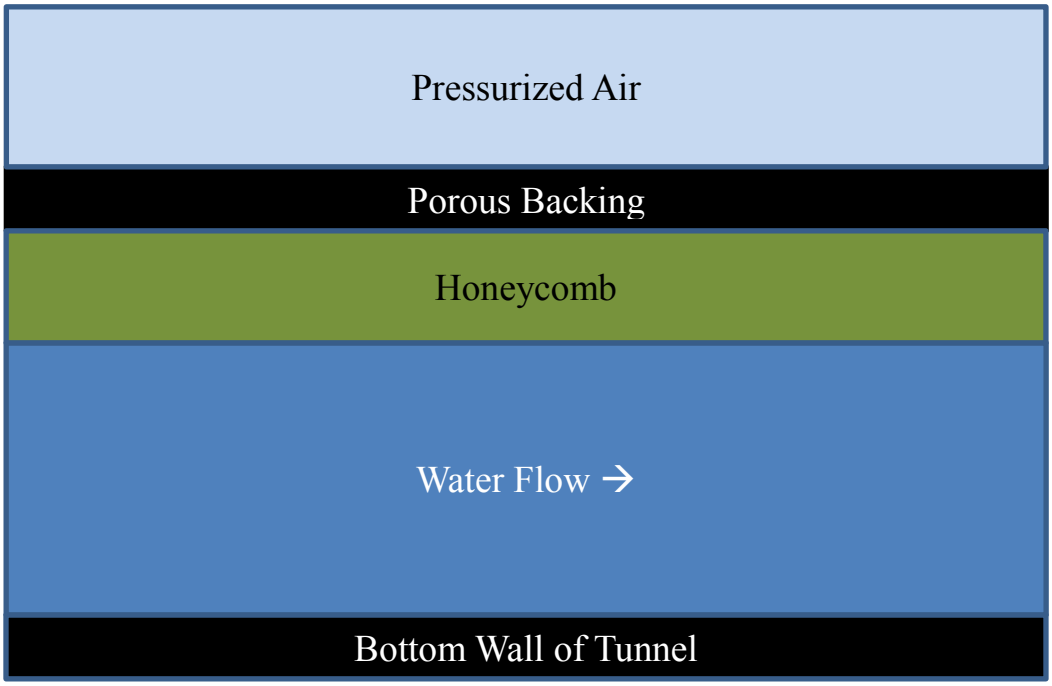

Figure 24: Honeycomb Test Apparatus Diagram

Figure 25: Honeycomb Testing Apparatus

Rather than placing the test surface on the bottom of the tunnel as in the previous cases, the honeycomb was installed as the ceiling of the tunnel. Also, the honeycomb wall was sealed to an acrylic/PVC backing that allowed a quantity of air to be pressurized in the middle. It was determined that the air would be pulled from this system as easily as that of the honeycomb board without the acrylic/PVC backing. Shop air was connected to the system in order to replenish the air lost as the water rushed past. The pressure of the shop air was controlled by a manual pressure regulator. The white hose at the top of the Figure 25 is connected to the pressure regulator. Both the pressure regulator and the height of the ceiling of the tunnel (the honeycomb) could be adjusted until a steady state system was reached. At steady state, bubbles are continuously fixed to the honeycomb. When the system reached this equilibrium, the testing was started. At the beginning of each test, both the test surface elevation and the pressure regulator needed to be readjusted in order to reach a steady state. Because of this, each test was not conducted at the same air pressure in the tunnel. The size of the static bubbles changed with each different test. This change in size was visually observed and recorded in an attempt to determine the effect of bubble size on the viscous drag.

The experimental procedure for the honeycomb tests was similar to that of the smooth and SLIP surfaces. However, because the honeycomb was on the roof, rather than the bottom wall, the laser setup was inverted. Rather than beginning at the bottom wall and moving up, the data collection began at the top wall and moved down. All of the test cases of the honeycomb were conducted at a free stream velocity of $U_e \sim 0.35$ m/s which yields a Re_τ of approximately

500. Six different cases were conducted with varying bubble sizes, and the results are discussed in Section 6 of this paper.

After the initial testing, it was determined that the honeycomb setup was not accomplishing its purpose. The honeycomb has a porous backing that rather than improving the air distribution throughout the honeycomb as was intended, actually produced a negative effect. The pores in the backing are smaller than the pores of the honeycomb and ended up restricting the air flow to particular pores in the honeycomb. A pattern matching that of the porous backing was visible throughout the testing. This pattern is shown in Figure 26, the tan and green surfaces are support structure of the water tunnel, and the grey surface is the honeycomb. The lighter colored pockets show where the air bubbles were during testing. The darker areas were filled with water. In addition to the pattern, the distribution of the air bubbles was not uniform throughout the honeycomb. The ceiling height and air pressure regulator could only produce the small pockets of bubbles shown in Figure 26. There were several of these pockets throughout the honeycomb. Measurements for the first set of tests were conducted over one of these pockets. The results of these tests are discussed in Section 6.

Figure 26: Porous Backing Pattern

In an attempt to improve the performance of the honeycomb, the testing section was changed for an additional round of testing. The acrylic/PVC pressure vessel was modified so that the incoming air was directed to only a 0.5 m portion of the honeycomb. This setup is shown in Figure 27. The 0.5 m long testing section is clearly marked by the grey colored sealant. The remaining honeycomb on the flow side, not shown in Figure 27, both upstream and downstream from this testing section, was covered with Mylar and performed as a smooth surface.

Figure 27: Testing Apparatus for Honeycomb II

After adjusting the ceiling height and pressure regulator, the new testing section showed improvement. On the initial run, a 0.15 x 0.20 m area was filled entirely with static bubbles. However, upon turning off the pressure and draining the tunnel, the honeycomb filled with water and additional runs were unsuccessful in obtaining the same bubble distribution. In an attempt to prevent water from filling the honeycomb pores in the test section, the Krytox oil from the SLIP surfaces was applied to the pores in the test section. This resulted in improved performance because the added hydrophobicity was enough to prevent the water from staying inside the honeycomb over a 0.08 x 0.20 m area of the test section. This is shown in Figure 28. Again, the lighter colored pores show the areas where the bubbles were. The left end was completely filled with bubbles up to the left edge of the test section. LDV measurements were taken at the downstream edge of the continuous bubble area, directly above the yellow marker in the figure. The pattern from the porous backing is again visible after the continuous bubble area.

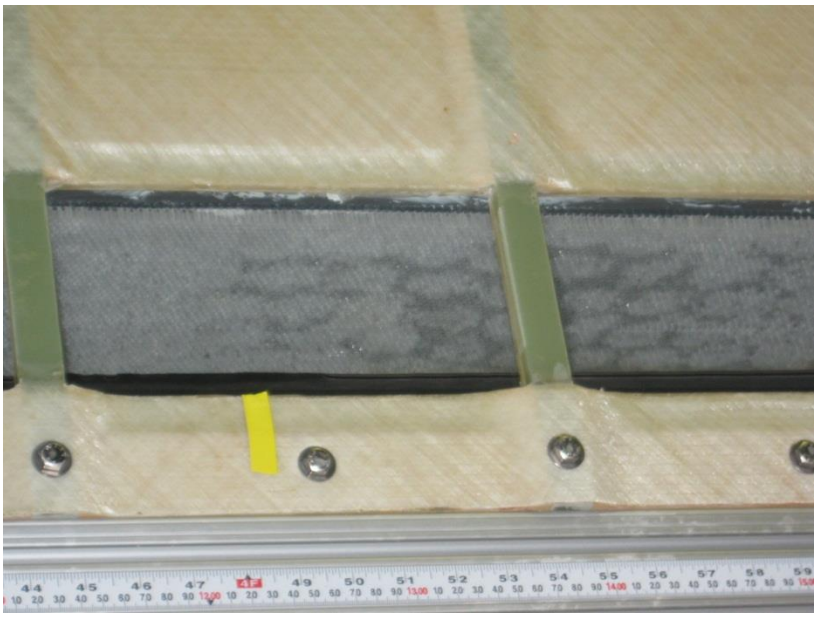

Figure 28: Honeycomb Bubbles II

Superhydrophobic Surface (SHS) Tests

The superhydrophobic surface was obtained from Professor Anthony Brennan at the University of Florida. Similar to the SLIP surface, the SHS was tested on the bottom wall of the water tunnel. The USNA workshop attached the SHS to an acrylic board using an adhesive. The prepared test surface is shown in Figure 29. Due to time constraints and expected performance based on work in the field, the SHS was only tested at the slowest speed, shown in Table 6, where the likelihood of success was highest.

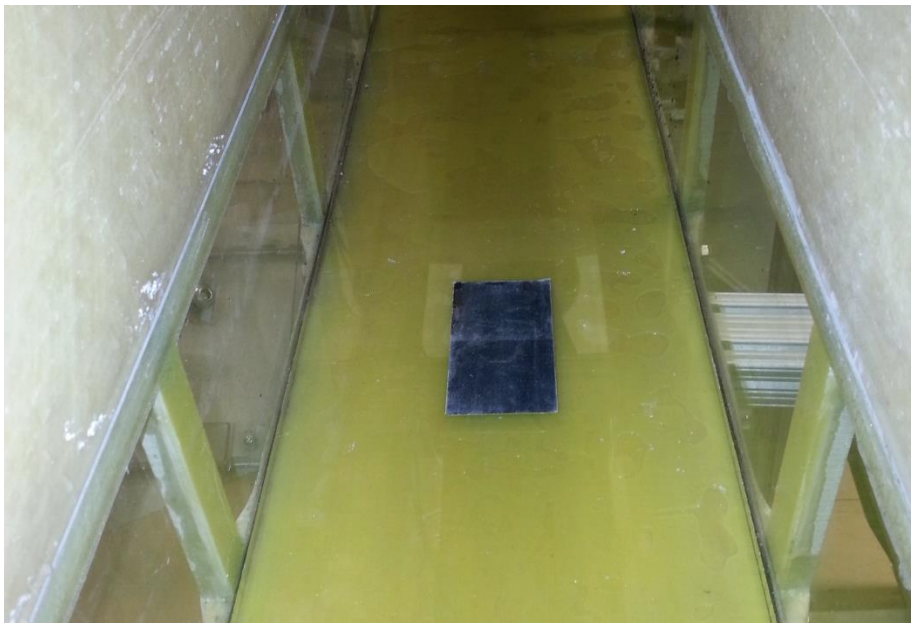

Figure 29: SHS in Water Tunnel

Table 6: SHS Test Matrix

	U_e (m/s)	Re_τ
Run 1	0.31	500

Figure 30 shows the SHS immediately after water has begun flowing over the surface. The sheen and the appearance of bubbles on the surface show that initially, air was trapped within the microstructures. However, visual observation determined that the majority of the air had been pulled from the surface within the first 30 minutes of being in the water tunnel. Figure 31 shows the same surface four hours later after the testing had been completed, still submersed in water, and no air is visible on the surface.

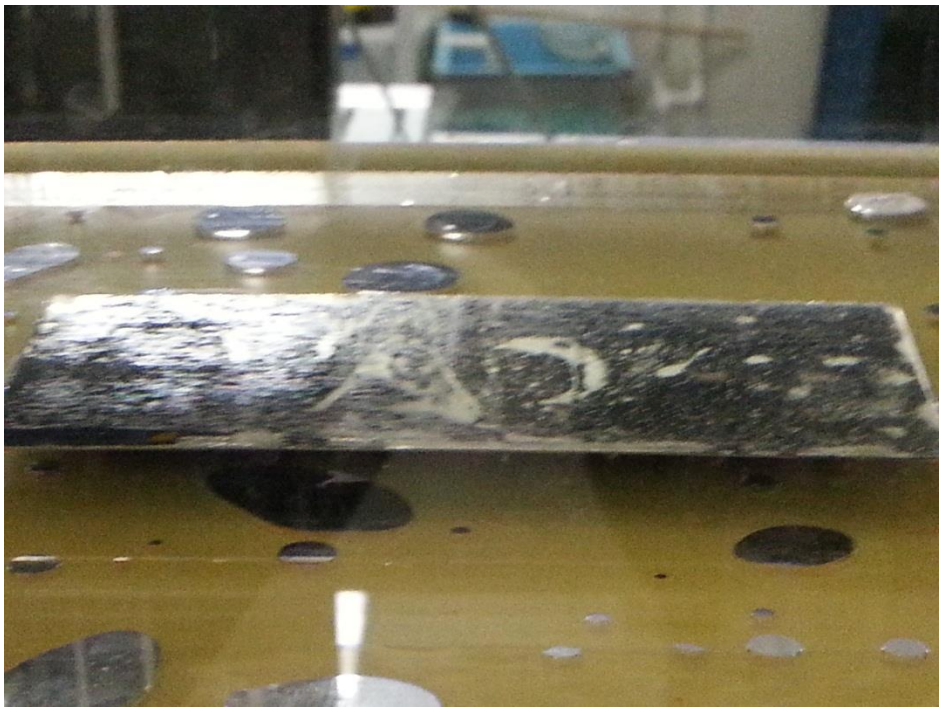

Figure 30: Initial Submersion of the SHS

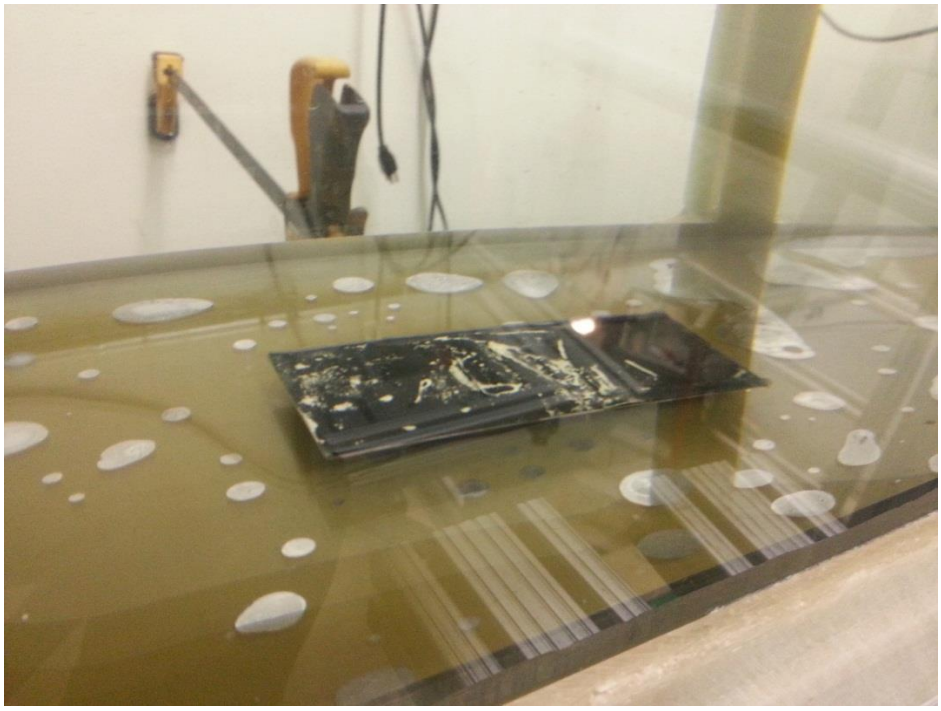

Figure 31: SHS after 4 Hours of Testing

Data Analysis

Normalized Velocity Plot

The objective of this project was to determine the effectiveness of the previously described surfaces at reducing drag in the turbulent boundary layer. The experiment was designed to gather enough data to characterize the velocity profile of the flow within the boundary layer. The velocity profile for a typical smooth surface is shown in Figure 32.

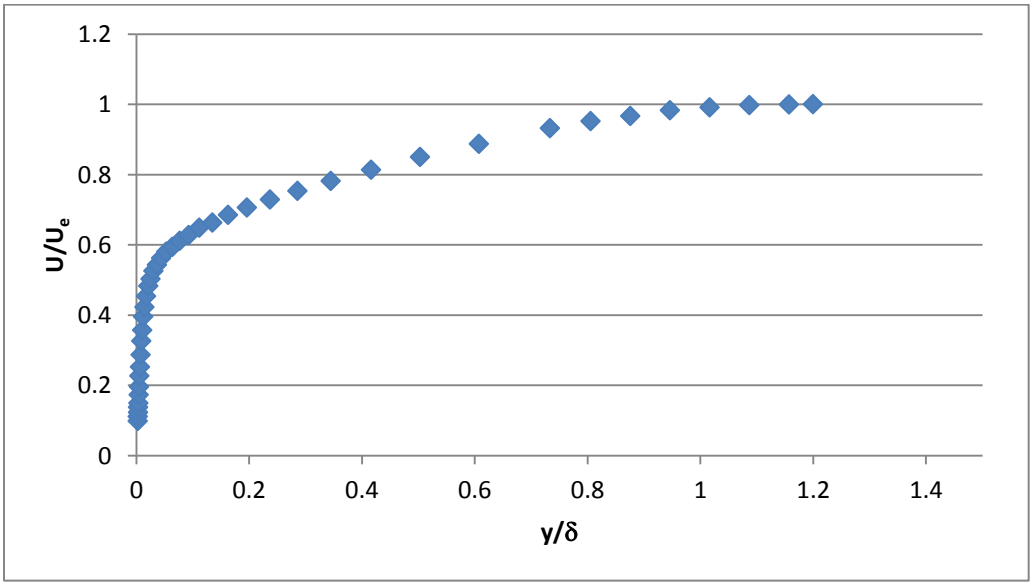

Figure 32: Smooth Wall Normalized Velocity Profile

The horizontal axis in this plot is the nondimensional displacement from the wall, given as the ratio of the actual position (y) of the measurement and the boundary layer thickness (δ). The vertical axis of the plot is defined to be the nondimensional velocity, given as the ratio between the velocity at a specific point (U) and the free-stream velocity (U_e). Comparison of the normalized velocity profile of a surface with that of the smooth wall under the same conditions can determine whether or not drag is being affected. For example, Figure 33 shows how an increase or decrease in drag would appear on the normalized velocity profile when compared to a smooth surface. If the drag were reduced, the fluid would be moving faster near the wall, thus resulting in a fuller plot; if the drag were increased, the fluid would be moving slower near the wall, thus resulting in a less full plot.

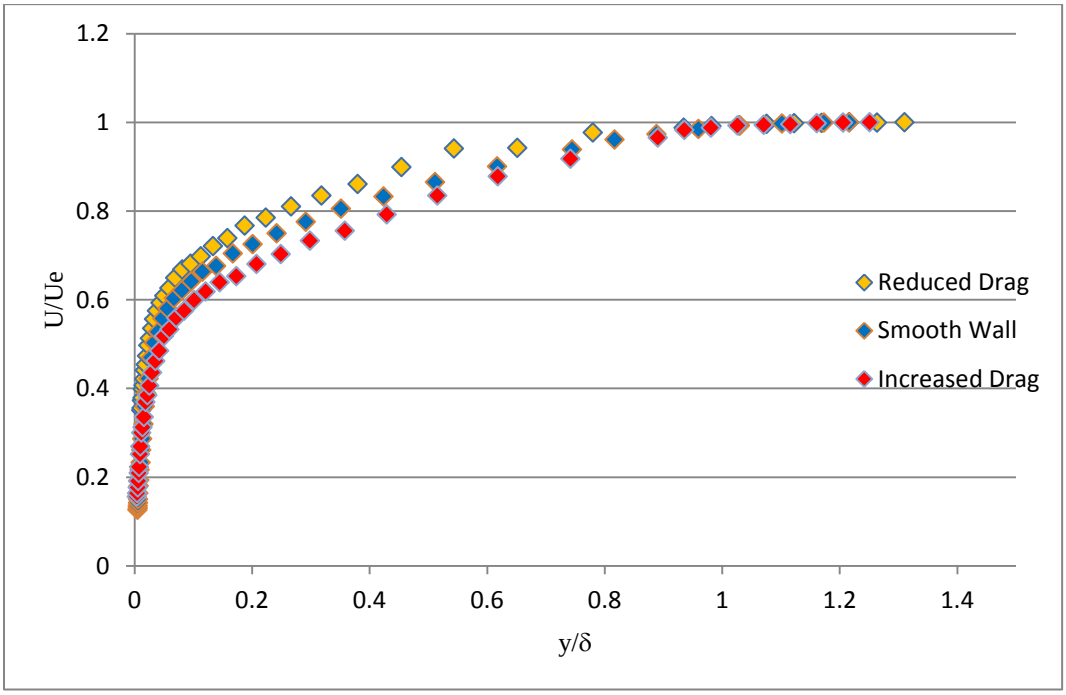

Figure 33: Effect of Drag on Normalized Velocity Profile

Reynolds Shear Stress (RSS) Analysis

The numerical analysis of the effect of the surface on the drag was conducted based on the Reynolds shear stresses (RSS) in the boundary layer. Essentially, Reynolds shear stress in the boundary layer is a result of turbulent mixing. Slower moving fluid close to the wall is "kicked up" into the faster moving fluid further from the wall and causes shear stress. The reverse is also true. The normalized Reynolds shear stress, given in Equation 4, nondimensionally quantifies the magnitude of the mixing that occurs. The numerator in this equation represents the mean value of the products of the fluctuations in velocity in the streamwise and wall normal directions. The u' and v' velocity components are in the streamwise and wall-normal directions, respectively. The over-bar indicates a time average of all the data acquired at a particular location in a test.

$$RSS = \frac{-\overline{u'v'}}{{u_\tau}^2} \qquad (4)$$

The friction velocity term (u_τ) in the denominator of Equation 4 is defined in Equation 5 as being dependent on the free-stream velocity (U_e) and the skin friction coeffiecient (c_f).

$$\frac{U_e}{u_\tau} = \sqrt{\frac{2}{c_f}} \tag{5}$$

Figure 34 is a plot of the RSS and its location in the boundary layer (y/δ). As shown in Figure 34, the peak of the RSS plot occurs around the value 1.0, regardless of any flow or surface characteristics. This RSS peak consistency was used to determine the skin friction drag coefficient for the surfaces tested in the experiment.

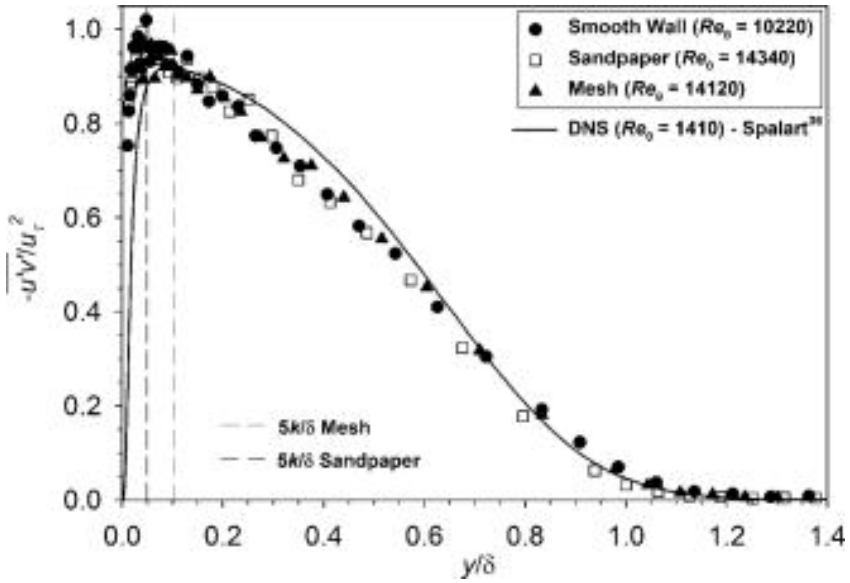

Figure 34: Reynolds Shear Stress Plot (Flack et al 2005)

6. Results and Discussion

Smooth Wall Tests

The normalized velocity profile for each Re_τ tested for the baseline smooth surface is shown in Figure 35. Essentially, all of the data follow the same curve, that of a smooth wall. This curve agrees with previously published data. These plots were used as the basis for comparison to determine the modified surfaces' effect on drag at specific Reynolds numbers.

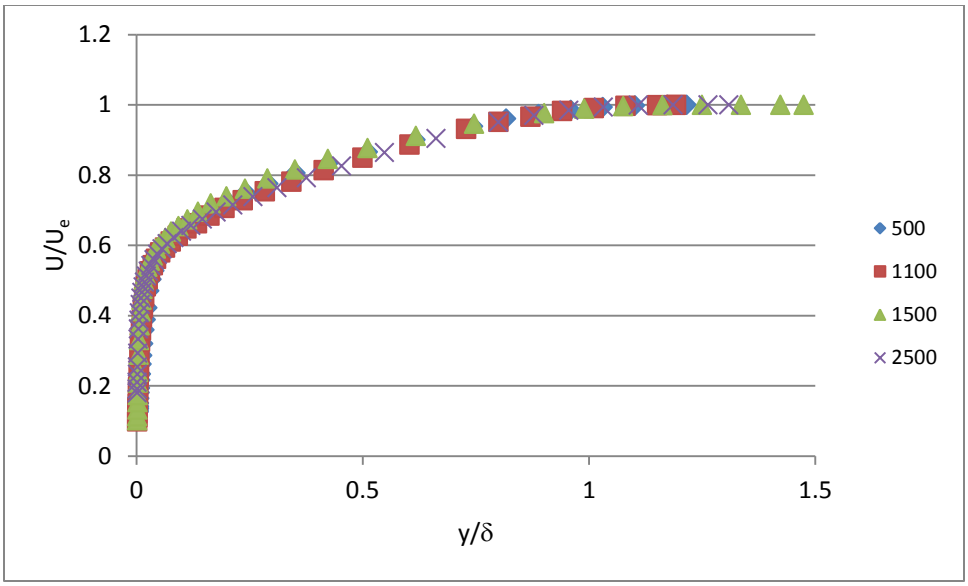

Figure 35: Smooth Wall, Normalized Velocity Plot

Figure 36 shows the Reynolds Shear Stress plots that were used to determine the skin friction coefficient, c_f. Table 7 shows the magnitude of the skin friction. The boundary layer thickness (δ) for each run is also included in the table. These values agree well with previously published data for turbulent boundary layer flow over a smooth wall.

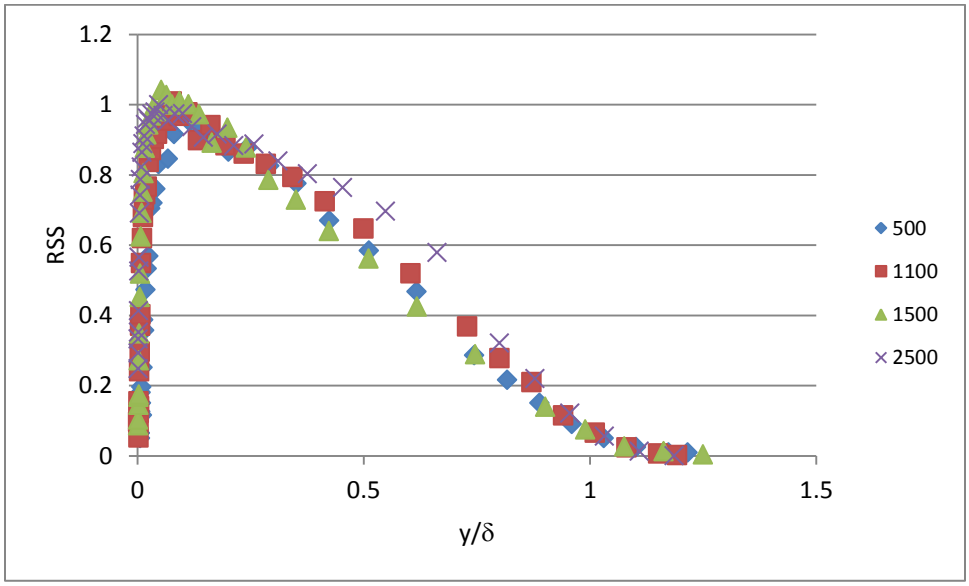

Figure 36: Reynolds Shear Stress Plot

Table 7: Results from Baseline Tests

	U_e (m/s)	Re_τ	c_f	δ (mm)
Run 1	0.32	530	0.0039	35.1
Run 2	0.78	1100	0.0031	35.7
Run 3	1.25	1500	0.0029	28.9
Run 4	2.25	2700	0.0025	32.5

Teflon SLIP Surface

The normalized velocity profiles for the Teflon 100a and 100b surfaces are shown in comparison with the smooth wall velocity profiles at different Reynolds numbers in Figures 37-40. Based on the graphical analysis, the surfaces appear to have no drag reducing effect; the Teflon 100a and 100b surfaces closely follow the smooth wall curve.

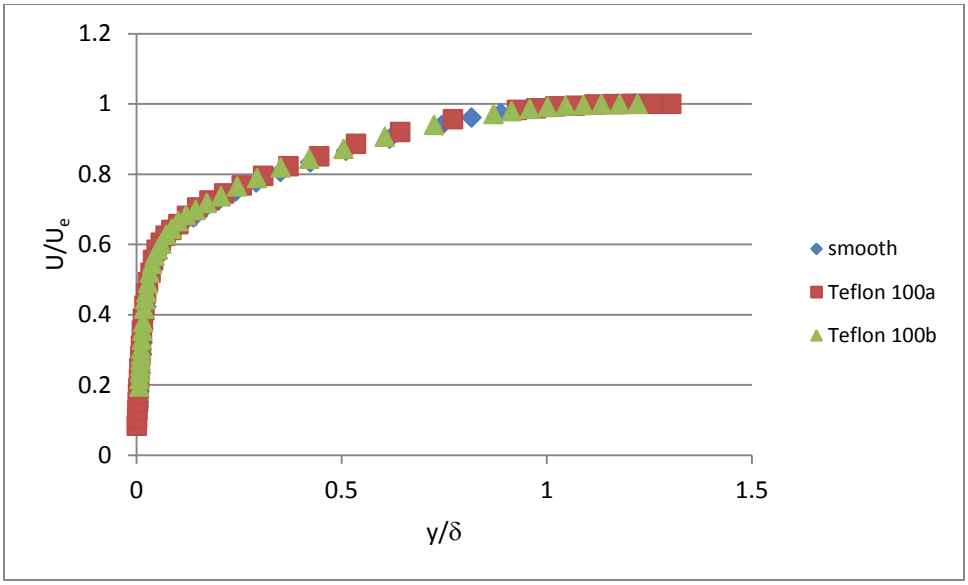

Figure 37: Teflon Comparison Plot, $Re_\tau = 500$

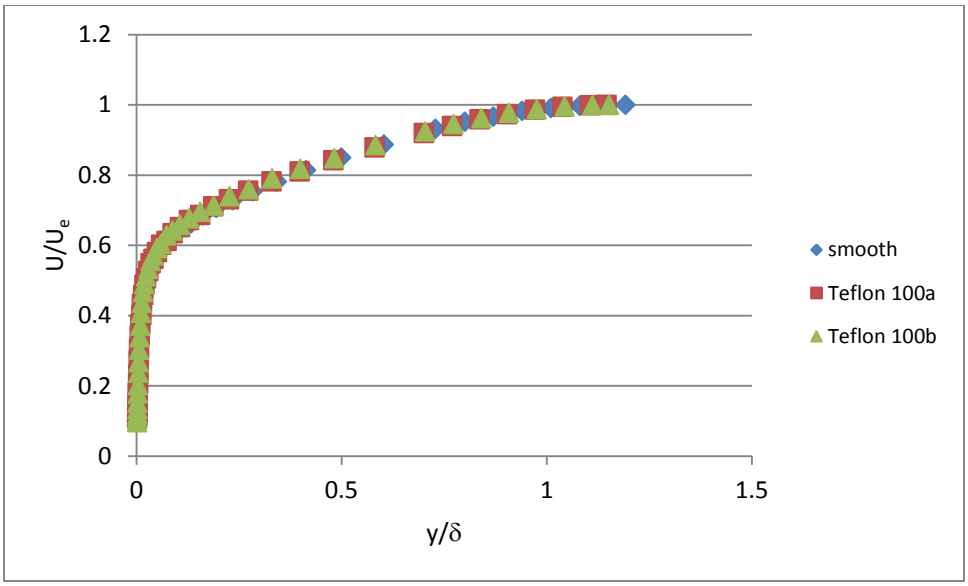

Figure 38: Teflon Comparison Plot, $Re_\tau = 1100$

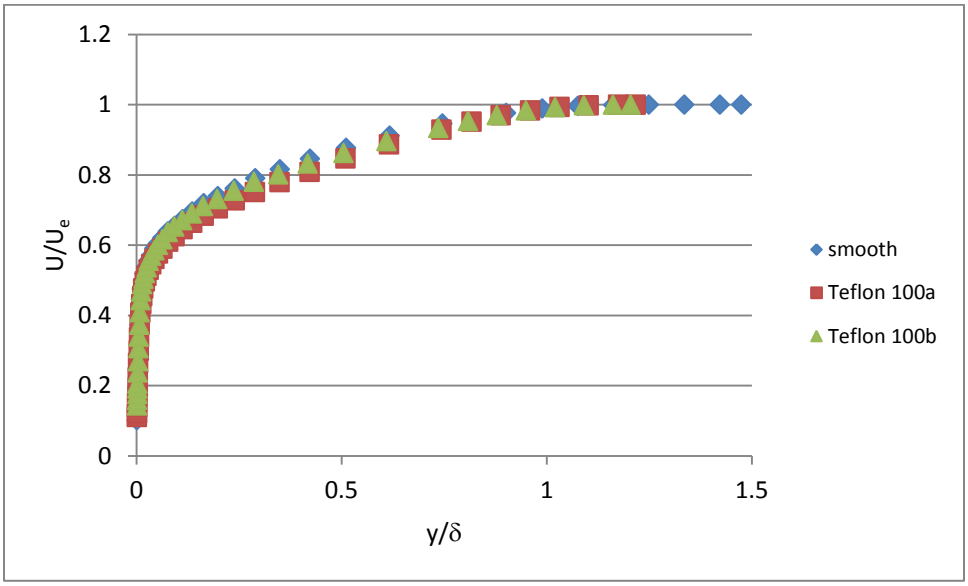

Figure 39: Teflon Comparison Plot, $Re_\tau = 1500$

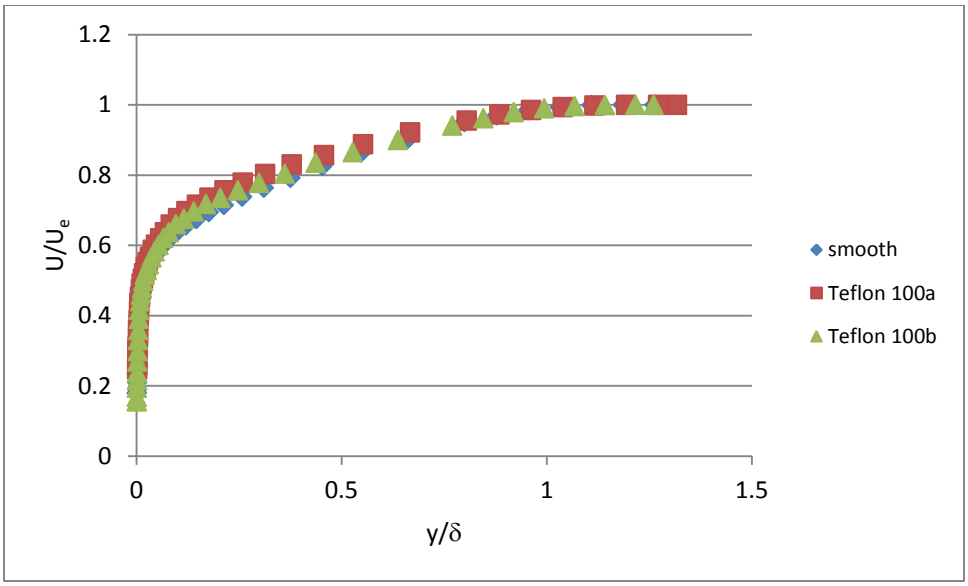

Figure 40: Teflon Comparison Plot, $Re_\tau = 2500$

Figures 41 and 42 shows the resultant RSS plots for each run in the Teflon 100a and 100b test matrices. The skin friction coefficient values and boundary layer thicknesses are included in Tables 8 and 9.

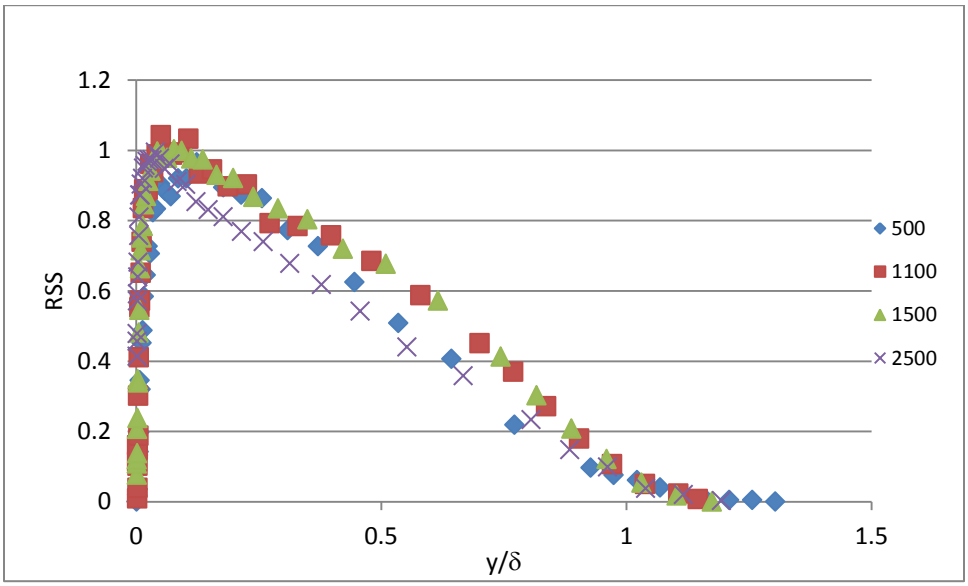

Figure 41: Teflon 100a RSS Plot

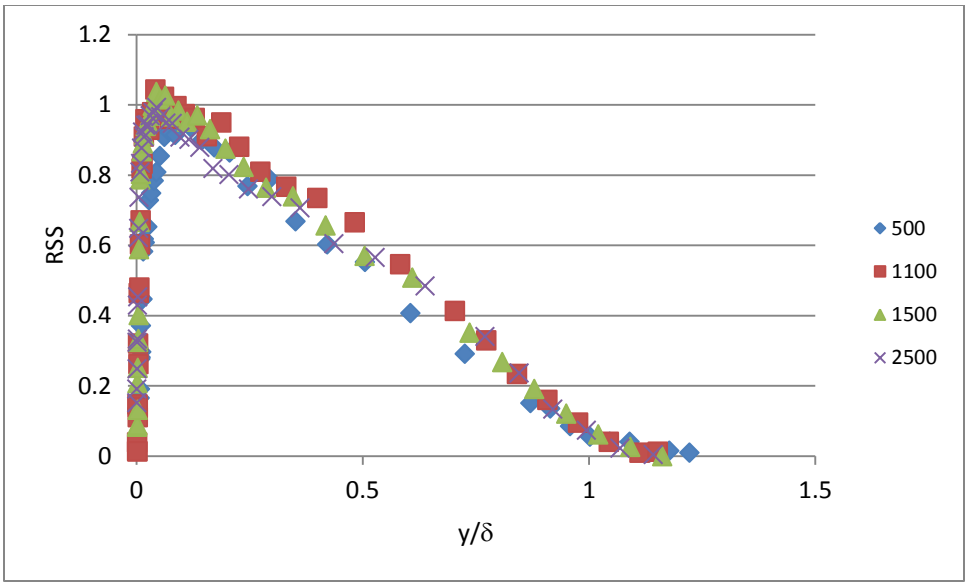

Figure 42: Teflon 100b RSS Plot

Table 8: Teflon 100a Results

	U_e (m/s)	Re_τ	c_f	δ (mm)
Run 1	0.32	500	0.0039	37.2
Run 2	0.78	1100	0.0030	37.2
Run 3	1.25	1500	0.0028	35.0
Run 4	2.25	2500	0.0028	32.3

Table 9: Teflon 100b Results

	U_e (m/s)	Re_τ	c_f	δ (mm)
Run 1	0.32	500	0.0040	39.9
Run 2	0.78	1100	0.0031	37.0
Run 3	1.25	1500	0.0028	35.4
Run 4	2.25	2500	0.0028	33.7

Teflon SLIP Observations

Based on the results obtained, the Teflon SLIP surface is not reducing drag. The comparisons of velocity profiles in Figures 37-40 nearly exactly follow the curve for a smooth surface. The values for c_f for runs 1-3 in Tables 8 and 9 are essentially equal to those of the smooth wall in Table 7, the small variations fall well within the experimental error. The increase in the c_f value in Tables 8 and 9 when compared to Table 7 indicates that the surface is actually increasing the drag at the highest Reynolds number in run 4.

The data also indicate that there is little relation between the amount of oil in the Teflon SLIP material and the flow characteristics. The c_f values in Tables 8 and 9 are the same, and the plots in both cases also appear very similar. Based on the results from the Teflon 100a and 100b tests, the amount of oil in the Teflon surface does not affect the flow. The consistency between the two cases shows that the SLIP surface is not accomplishing its purpose of creating slip in the

bulk fluid at the wall. If the oil were effective, the c_f values in Table 9 would be significantly different from those in Table 7.

Based on the results, it is apparent that not only were the Teflon SLIP surfaces ineffective at reducing drag, but that as the speed of the flow increased, the Teflon SLIP surface was negatively affecting the flow. Figures 43-46 are logarithmic plots of the normalized mean-square velocity fluctuations in the streamwise direction, $\overline{U'^2}^+$, for each of the different Re_τ tested. The horizontal axis is defined in Equation 6 as the nondimensional displacement from the wall with respect to the viscous length scale ν/u_τ. In this equation, ν represents the kinematic viscosity of the fluid.

$$y^+ = \frac{y u_\tau}{\nu} \qquad (6)$$

At the higher turbulence levels, shown in Figure 46, the peak of the Teflon SLIP surface begins to significantly vary from that of the smooth wall. As the speed of the flow increases, the viscous length decreases, meaning that surface imperfections unnoticed at lower Reynolds numbers will begin to appear. The decrease in the peak of the normalized mean-square velocity fluctuations indicates an increase in surface roughness. This relationship is more evidence that the theoretical water-oil boundary is not being created and that the texture of the Teflon SLIP surface is negatively affecting the flow. This also accounts for the increase in the c_f value seen at the higher Re_τ.

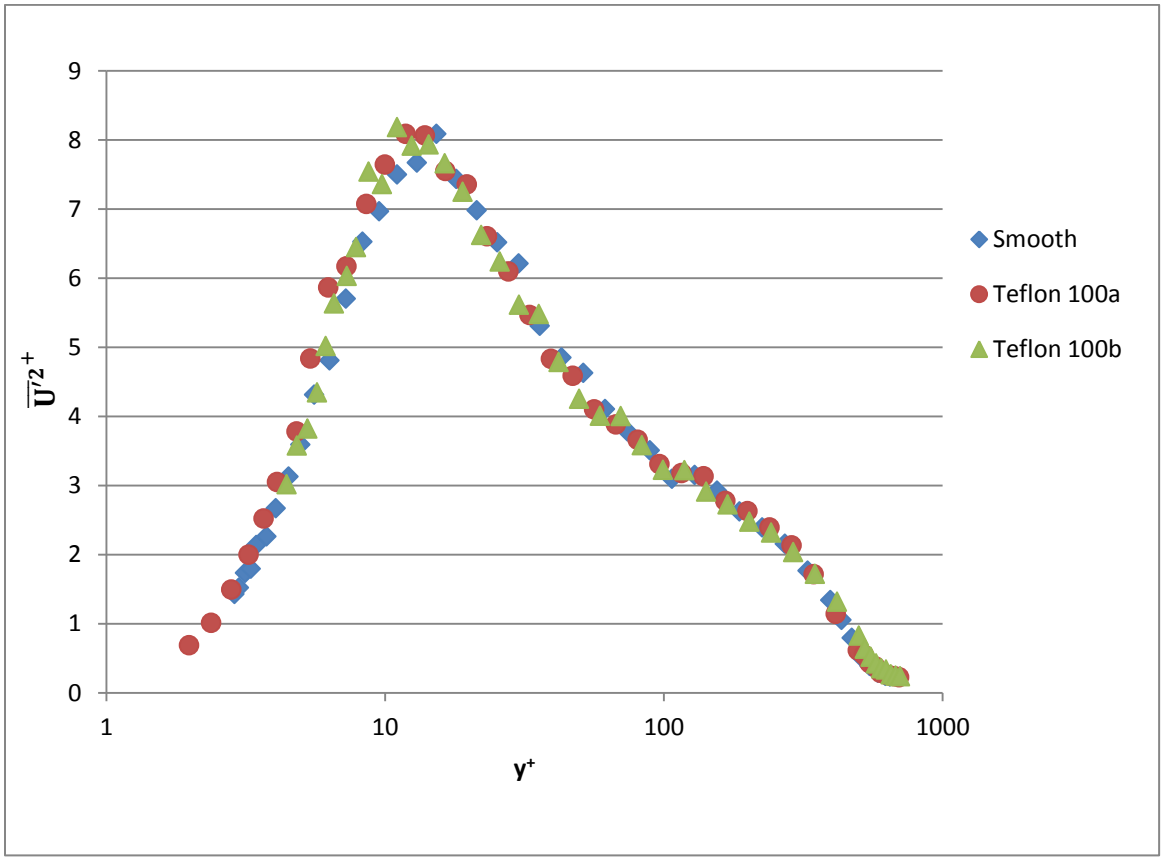

Figure 43: Normalized U', Inner Scaling, $Re_\tau = 500$

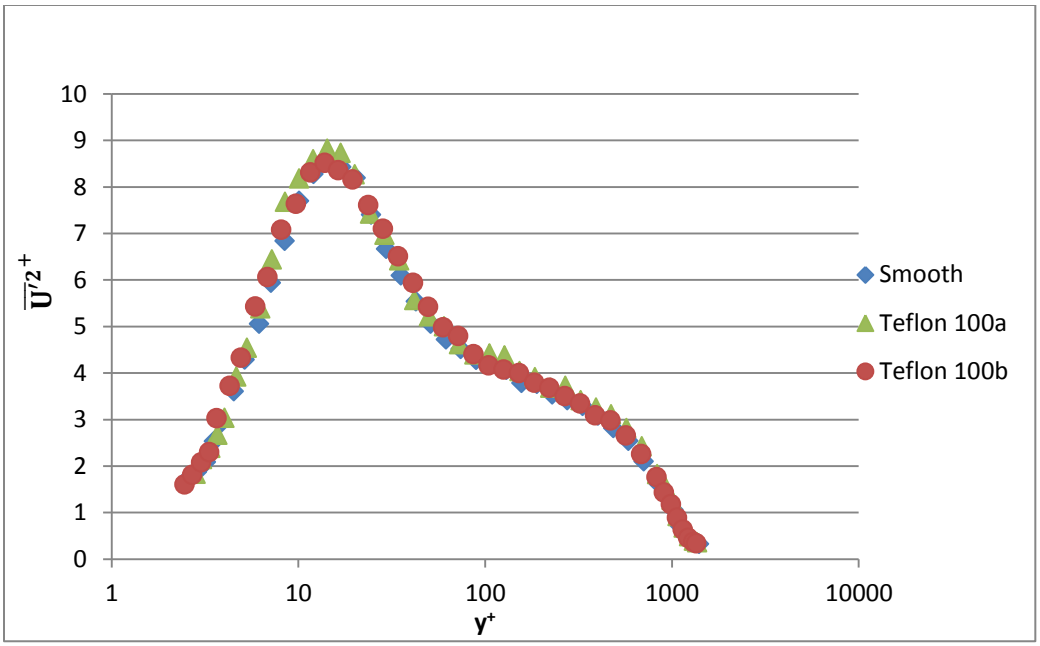

Figure 44: Normalized U', Inner Scaling, $Re_\tau = 1100$

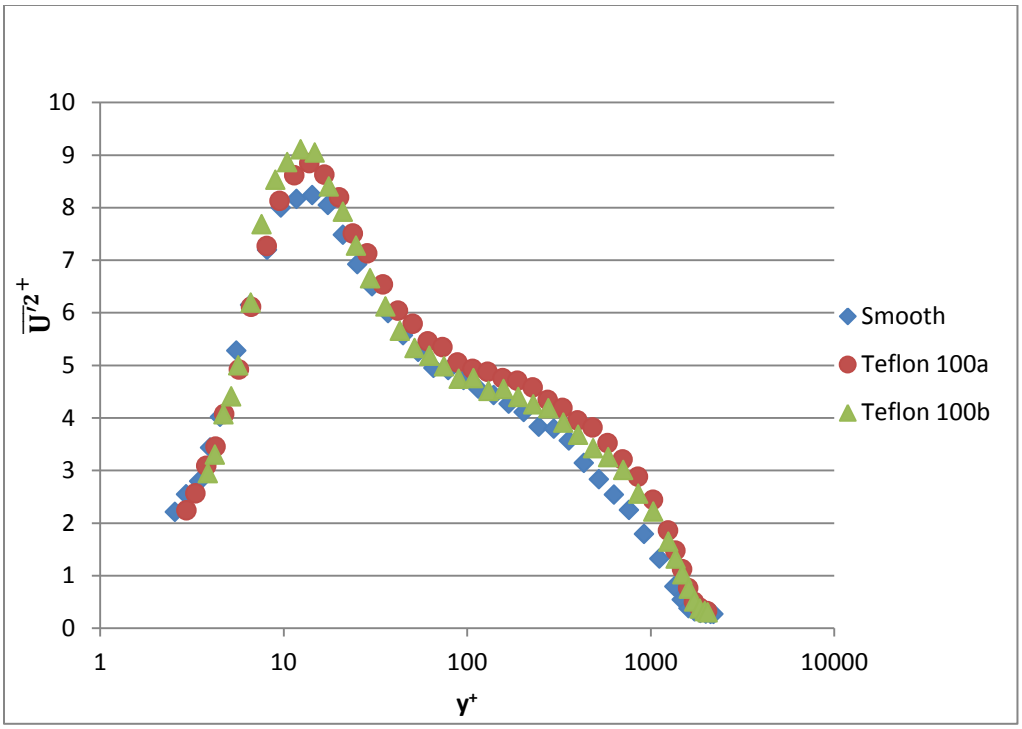

Figure 45: Normalized U', Inner Scaling, $Re_\tau = 1500$

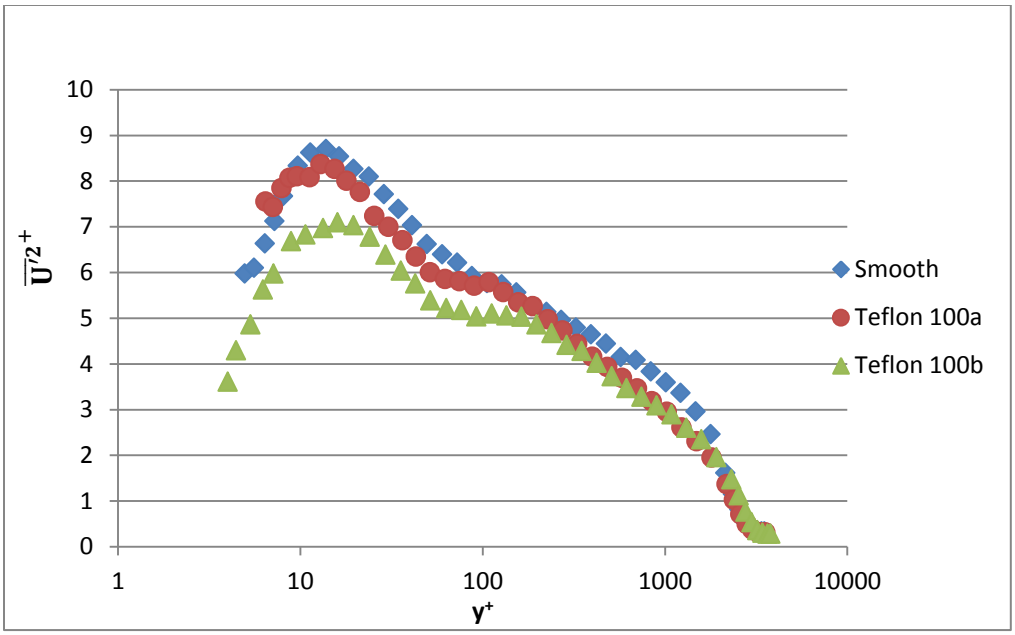

Figure 46: Normalized U', Inner Scaling, $Re_\tau = 2500$

Aluminum SLIP Surface

As mentioned previously, the Al SLIP surfaces were only tested at two medium Reynolds numbers, $Re_\tau = 1100$ and $Re_\tau = 1500$. The normalized velocity profiles for the Al 100, Al 102, and Al no oil surfaces are shown in comparison with the smooth wall velocity profile in Figures 47 and 48. Based on the graphical analysis, the surfaces appear to have no drag reducing effect; the Al 100, Al 102, and Al no oil surfaces closely follow the smooth wall curve.

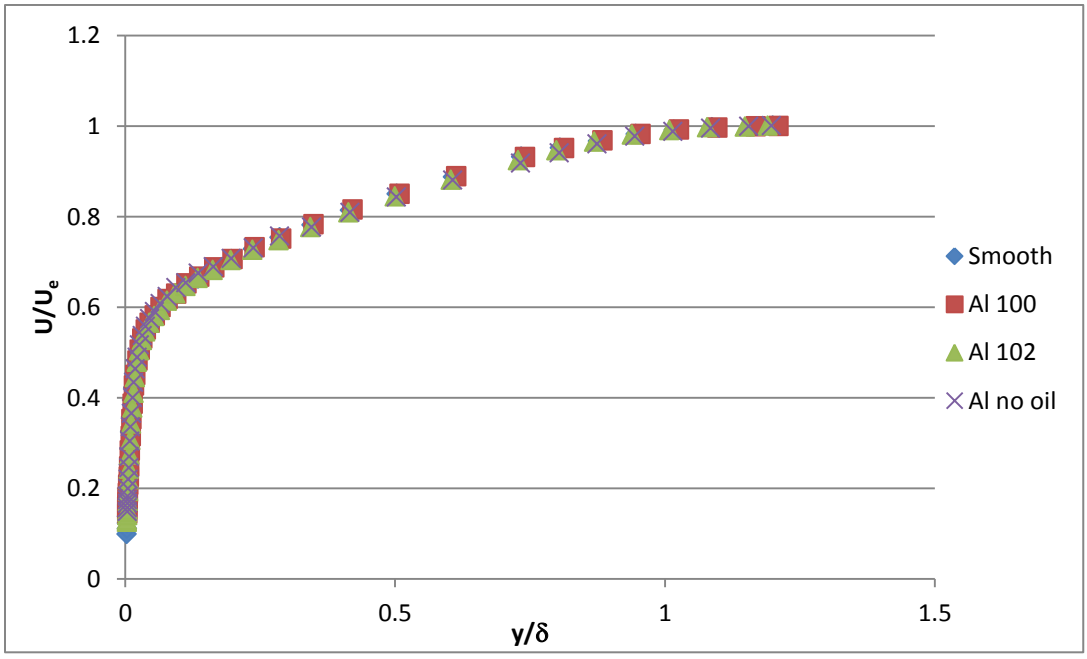

Figure 47: Al SLIP Comparison Plot, $Re_\tau = 1100$

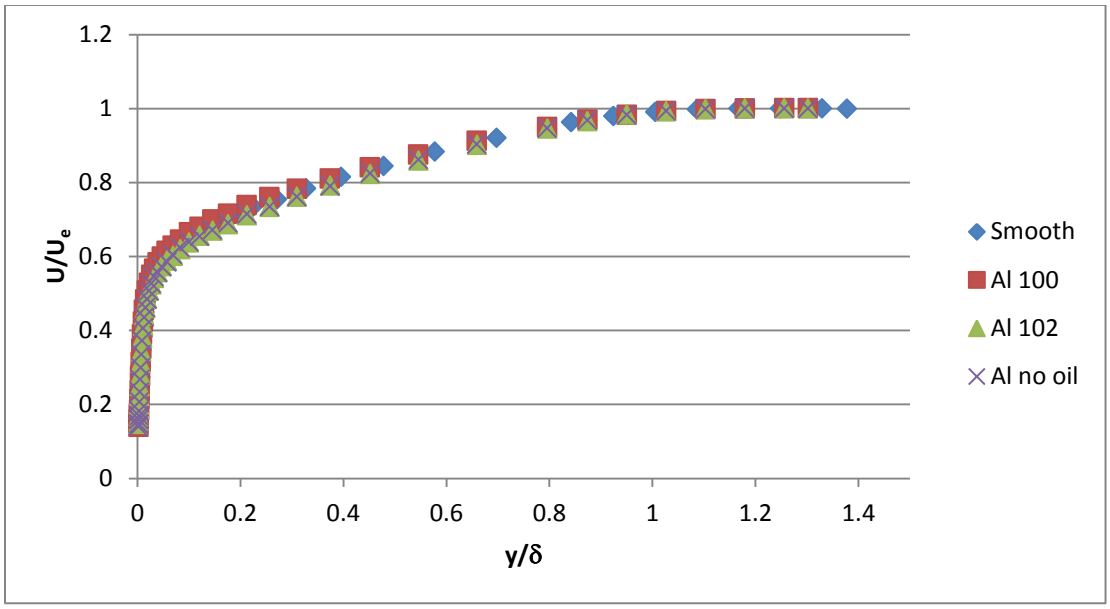

Figure 48: Al SLIP Comparison Plot, $Re_\tau = 1500$

Figures 49 and 50 show the resultant RSS plots for each run in the Al SLIP test matrices. The skin friction coefficient values and boundary layer thicknesses are included in Tables 10-12.

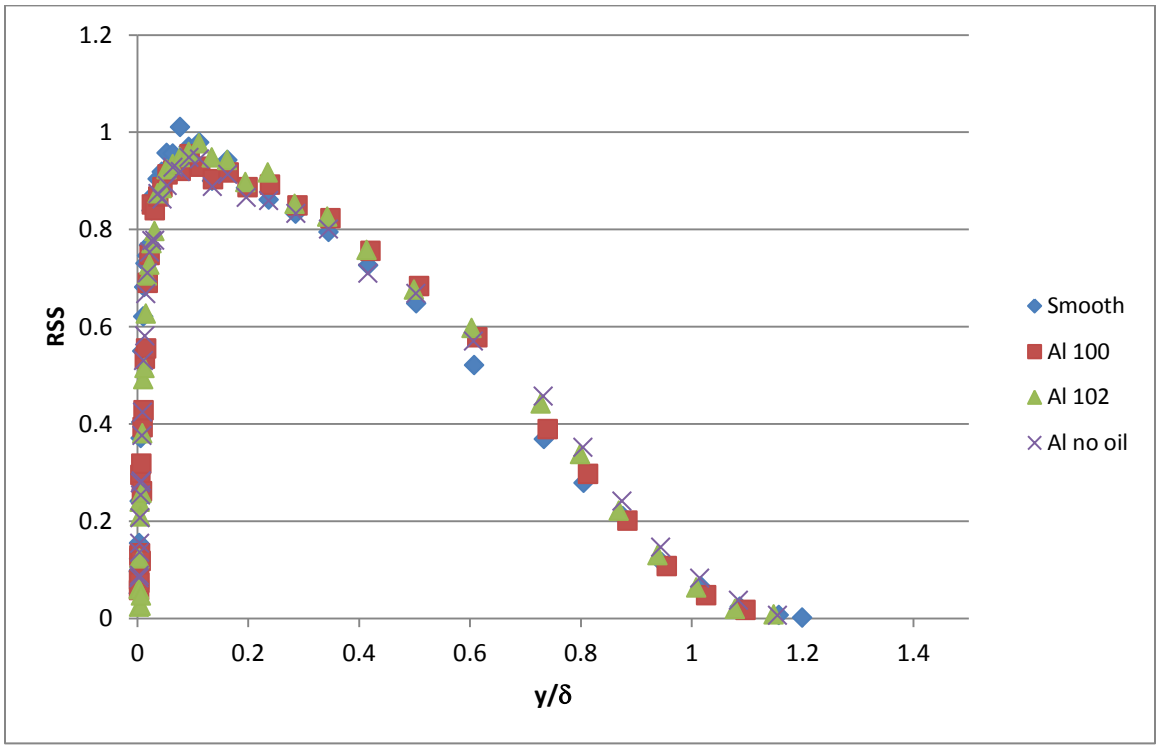

Figure 49: Al SLIP surface RSS Plot, $Re_\tau = 1100$

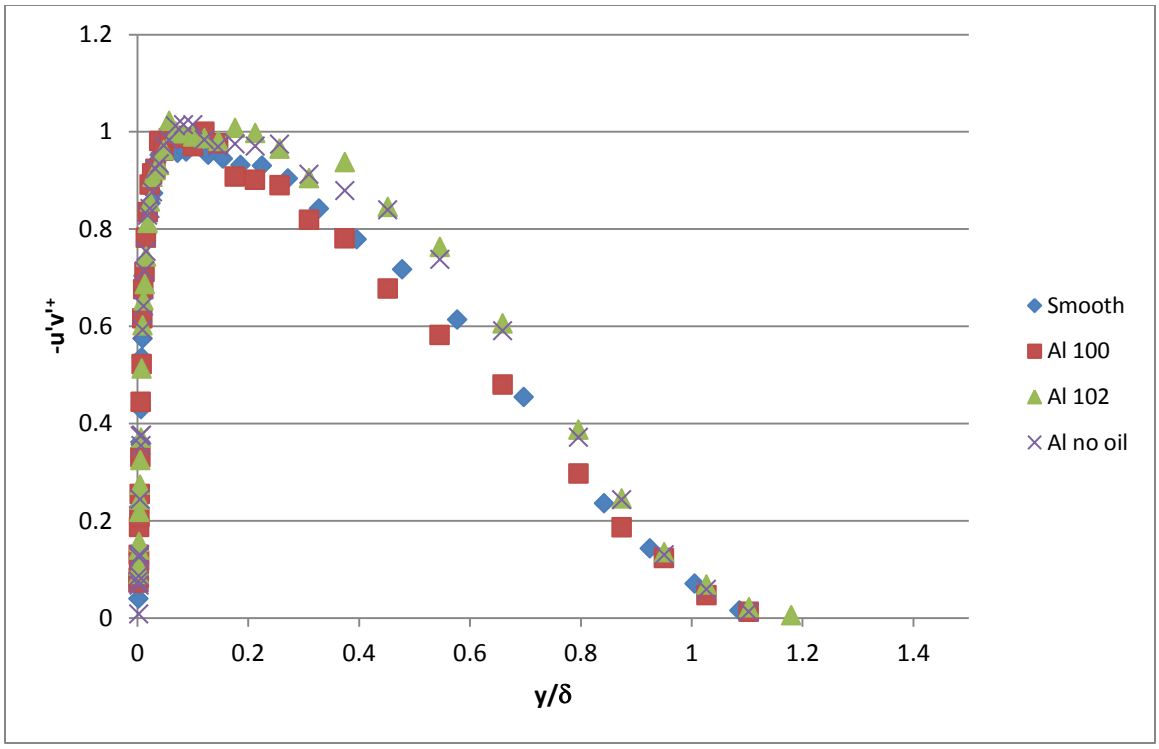

Figure 50: Al SLIP surface RSS Plot, $Re_\tau = 1500$

Table 10: Al 100 Results

	U (m/s)	**Re_τ**	**c_f**	**δ (mm)**
Run 1	0.78	1100	0.0031	35.2
Run 2	1.25	1500	0.0029	32.7

Table 11: Al 102 Results

	U (m/s)	**Re_τ**	**c_f**	**δ (mm)**
Run 1	0.78	1100	0.0031	35.8
Run 2	1.25	1500	0.0028	32.7

Table 12: Al no oil Results

	U (m/s)	**Re_τ**	**c_f**	**δ (mm)**
Run 1	0.78	1100	0.0031	35.6
Run 2	1.25	1500	0.0028	32.7

Aluminum SLIP Observations

Based on the data gathered throughout the experiment, the Aluminum SLIP surface has no effect on the drag over the wall. The velocity profiles in Figures 47 and 48 show that the Al SLIP surfaces behave as a smooth wall at the Reynolds numbers that were tested. The results shown in Tables 10-12 provide c_f values that are equal to those obtained for the smooth wall in Table 7. Because there was no evident drag reducing effect on the flow, the higher Reynolds numbers were not tested. Based on the analysis of the Teflon SLIP surface, the Aluminum SLIPS

performance is predicted to decrease at higher Re_τ. Due to the nano-scale of the surface features and the micro-scale of the viscous length, roughness was not evidenced in the Al SLIP surface tests.

The data indicate that either the desired water-oil surface was not created, or that it may have existed but due to the relationship between the surface features and the viscous length scale, nano vs. micro, it was unable to significantly affect the flow. Regardless, the Aluminum SLIP surface is ineffective at reducing drag under the conditions tested.

Honeycomb Surface

For the honeycomb test matrix, run 1 was taken with the initial configuration discussed in Section 5. Runs 2-6 were taken with the modified section after applying the Krytox oil. The data analysis was conducted in the same manner as both the baseline and SLIP surface cases. Figure 51 shows the normalized velocity profiles for the honeycomb experiment compared with that of the smooth wall. The RSS plot used to determine c_f is included in Figure 52. The numerical results for the honeycomb surfaces are shown in Table 13.

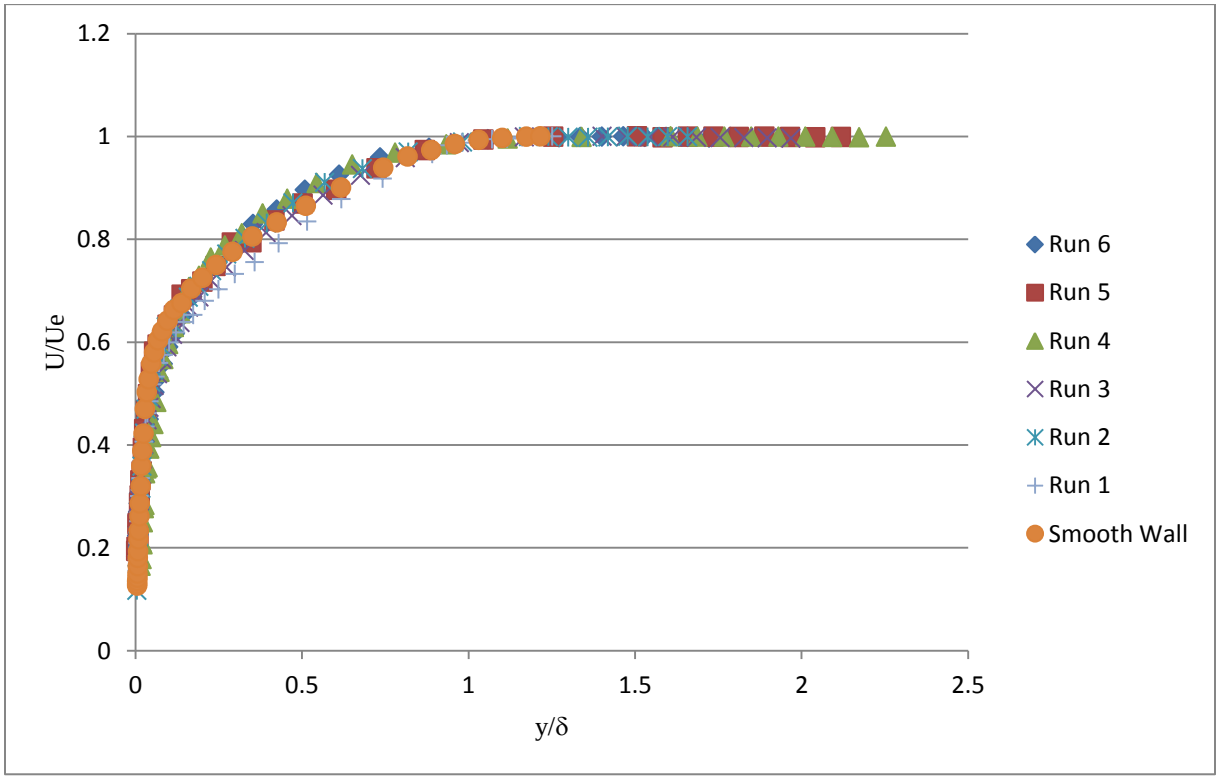

Figure 51: Honeycomb Comparison Plot, $Re_\tau \sim 500$

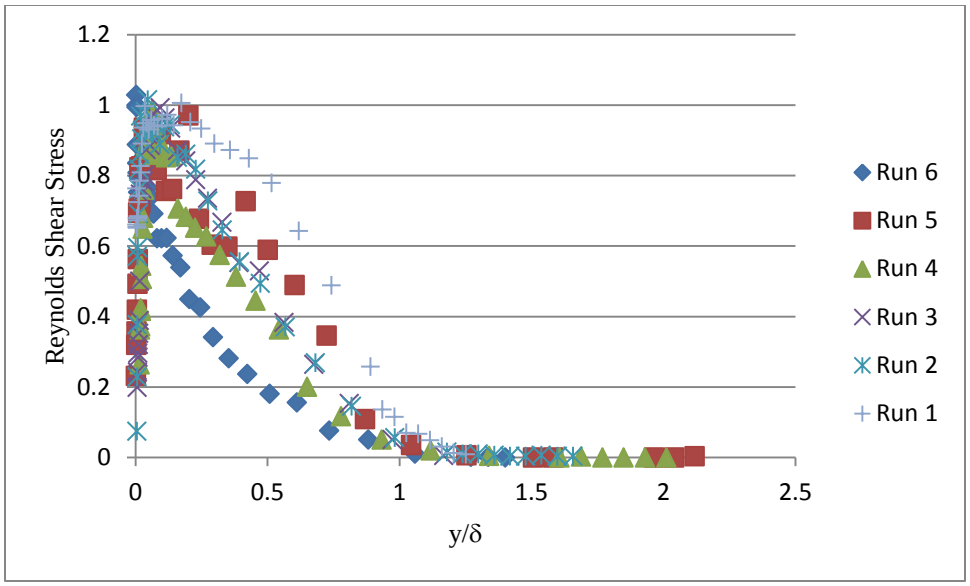

Figure 52: Honeycomb RSS Plot, $Re_\tau \sim 500$

Table 13: Honeycomb Results

	U_e (m/s)	Re_τ	c_f	δ (mm)
Run 1	0.356	670	0.0052	38.9
Run 2	0.343	510	0.0055	29.3
Run 3	0.356	460	0.0065	24.7
Run 4	0.354	430	0.0073	21.7
Run 5	0.352	400	0.0055	22.9
Run 6	0.366	700	0.0110	27.2

Honeycomb Surface Observations

The data indicate that the honeycomb surface is not effective at reducing drag. Comparison of the honeycomb c_f values in Table 13 with those of the smooth wall in Table 7 shows that the honeycomb material is significantly increasing the viscous drag in the flow. Also, there is no apparent difference in the performance of the initial test section, run 1, and the modified test section with the Krytox oil, runs 2-6. However, the most notable trend in the honeycomb results is the variability between each of the different cases. Comparison of the Re_τ, c_f, and δ values for each run shows little similarity. Repeatability with the testing apparatus was not achievable. As mentioned in Section 5, each test run was conducted over bubbles of different sizes at different locations in the flow. The changes were not drastic but, as shown in Table 13, the effect on the results is evident. It is possible that the honeycomb surface is not reducing drag because the apparatus was not properly configured.

For example, Figure 52 shows the Reynolds shear stress plots for runs 1-6. Comparison of the individual runs shows that there is a noticeable difference in the consistency of data being captured; the plot for each run has a different shape. When compared with the plots of the previous testing sets of the smooth surface in Figure 36, the Teflon SLIP surface in Figures 41 and 42, and the Aluminum SLIP surfaces in Figures 49 and 50, it is evident that the honeycomb results are inconsistent both from one run to the next and with previously obtained data.

The data also indicate that the surface roughness of the honeycomb has a large impact on the flow. Figure 53 is a logarithmic plot of the normalized mean-square velocity fluctuations in the streamwise direction and the normalized displacement from the wall. The data in this plot came from the baseline smooth wall case, run 1, and the honeycomb case, run 1. It is clear by the 25% decrease in peak magnitude that the roughness of the honeycomb is affecting the flow. The goal of maintaining a layer of air between the honeycomb and the water was not accomplished in this experiment.

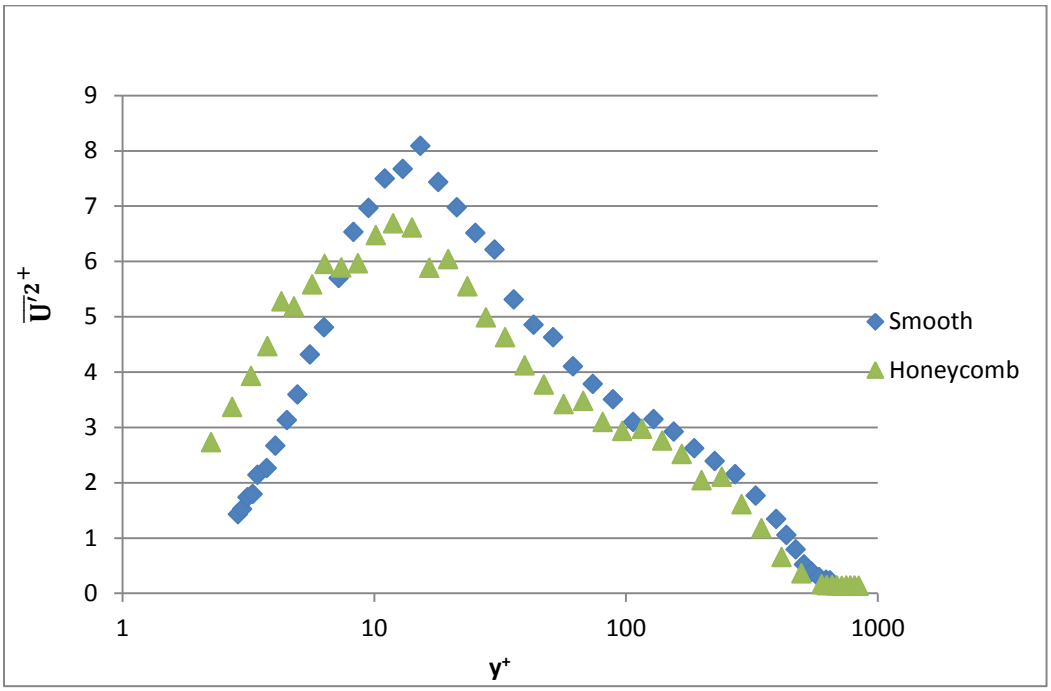

Figure 53: Normalized U', Inner Scaling, $Re_\tau = 500$

Superhydrophobic Surface (SHS)

As mentioned previously, the SHS was only tested at one Reynolds number, Re_τ=500. The normalized velocity profiles for the SHS is shown in comparison with the smooth wall velocity profile in Figure 54. Based on the graphical analysis, the surface appears to have no drag reducing effect; the SHS profile closely follows the smooth wall curve. Figure 55 shows the RSS plot that was used to determine the values shown in Table 14.

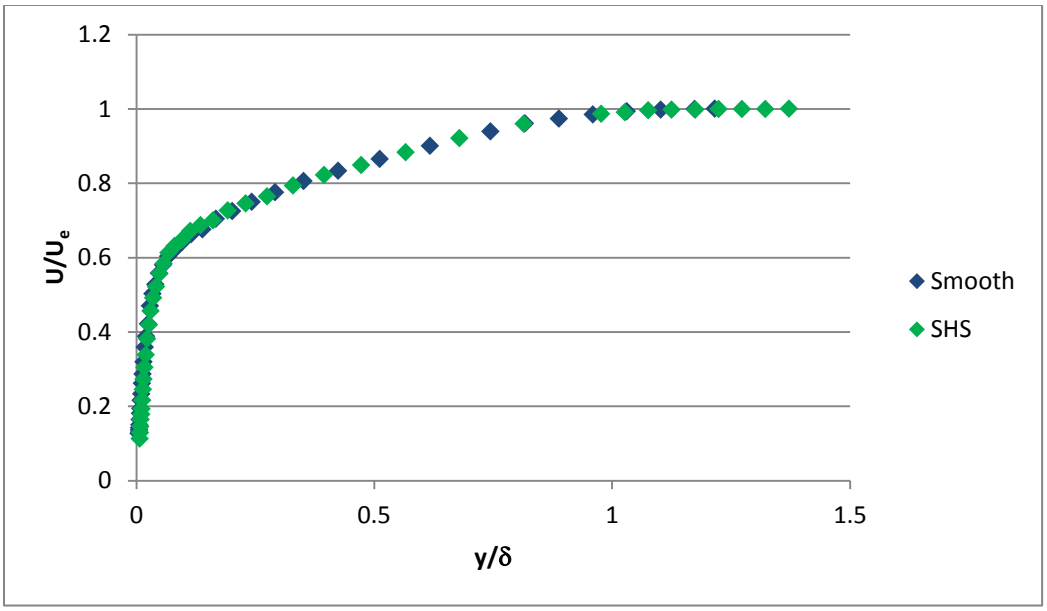

Figure 54: SHS Comparison Plot, $Re_\tau \sim 500$

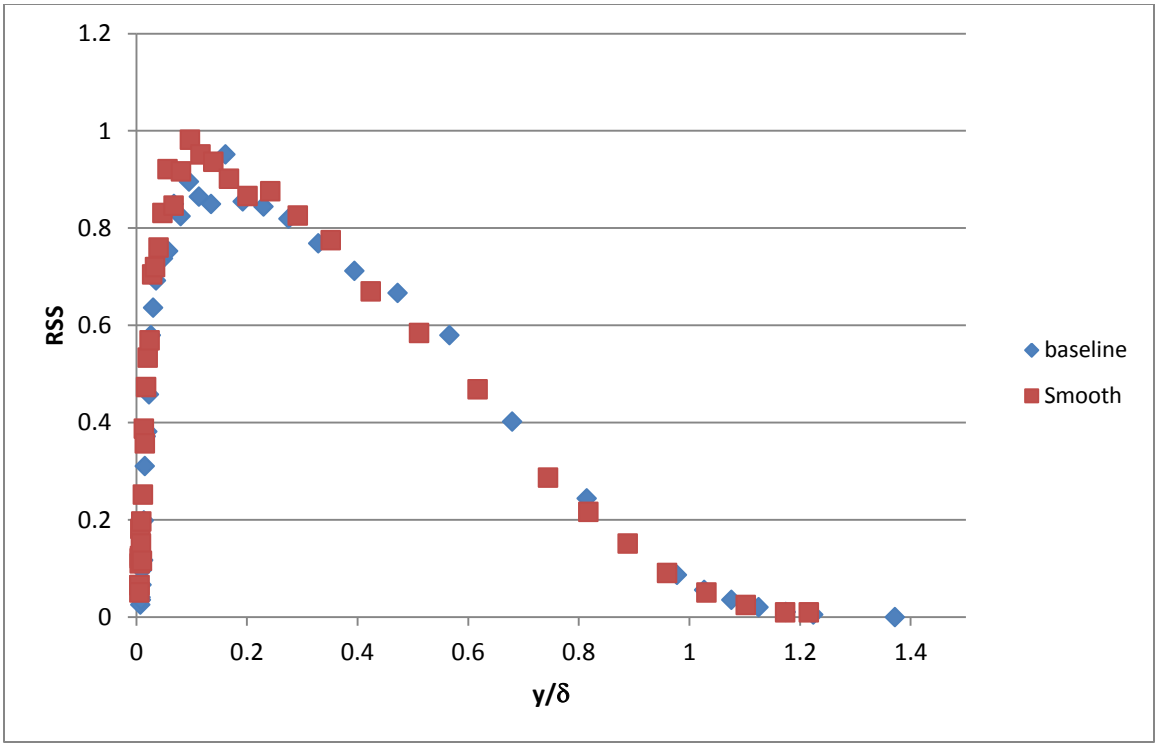

Figure 55: SHS RSS Plot, $Re_\tau \sim 500$

Table 14: SHS Numerical Analysis

	U_e (m/s)	Re_τ	c_f	δ (mm)
Run 1	0.32	500	0.0039	35.5

SHS Observations

Based on the data gathered throughout the experiment, the SHS surface has no effect on the drag along the wall. The velocity profile in Figure 40 shows that the SHS surface behaves as a smooth wall at the Reynolds number tested. The results shown in Table 14 provide a c_f value equal to that obtained for the smooth wall in Table 7. Because there was no evident effect on the flow, additional tests were not conducted. Based on the gathered data and visual observation, the surface is unable to retain the water-air interface that is necessary to reduce the drag in the flow. At the Reynolds number tested, there was no indication of surface roughness having any effect on the flow.

7. Conclusions

Smooth Wall

- The data obtained for the smooth wall agreed with published values.
- The data could accurately be used in comparison with the modified surfaces to determine their effect on drag.

Future work: N/A

Teflon SLIPS

- The Teflon SLIPS showed no indication of drag reduction.
- The velocity profiles at low and intermediate Reynolds numbers closely matched those of a smooth wall.
- At high Reynolds numbers, the effect of the roughness of the Teflon surface increased the drag in the flow.

Future work: It is not recommended that future work in the area of drag reduction be conducted on the Teflon SLIP surfaces.

Aluminum SLIPS

- The Aluminum SLIPS showed no indication of drag reduction.
- The velocity profiles at the Reynolds numbers tested closely matched those of a smooth wall.
- Although not tested, the data predict that the Aluminum SLIP surfaces will not be effective at low and high Reynolds numbers.

Future work: It is recommended that changes to the nanoscale porous layer be made to improve performance. It is possible that the current "random" boehmitization of the porous layer could be reducing the effective slip length. It is recommended that the porous layer be ordered, similar to that of the PDMSe superhydrophobic surface.

Honeycomb

- The honeycomb surfaces significantly increased the drag in the flow.
- A uniform steady state testing condition was never reached.

Future work: It is recommended that the testing apparatus for the honeycomb surface be improved. Specifically, the porous backing on the honeycomb layer should be removed, thus removing the previously mentioned "pattern" that influenced the formation of the bubbles. Also, changes could be made to improve the manner in which air is introduced into the system. Multiple air compressors and pressure regulators could be used to provide a more even distribution of flow. A larger, uniform test section may have a larger impact on the flow.

PDMSe SHS

- The superhydrophobic surface showed no indication of drag reduction.
- The surface performed as a smooth wall.
- Although not tested, the data predict that the superhydrophobic surface would not be effective at higher Reynolds numbers.

Future work: It is recommended that the microfeatures of the surface be adjusted. Throughout the testing process, the air was getting pulled out of the longitudinal microridges. Latitudinal barriers (on the same scale as the microridges) may be effective at retaining the air.

Summary

Although none of the tested surfaces proved successful at reducing drag in turbulent boundary layer flow, the research was effective in accomplishing its objective: obtaining a deeper understanding of how these surfaces perform in the specific conditions. The data, analysis, and recommendations provided through this study can be used to direct future work in the area of modified surfaces. For example, adapting the microfeatures on the SHS may be effective at reducing the amount of air that is lost and thus increase surface's performance. Also, introducing a hierarchical order to the SLIP porous network, such as the mountain-valley pattern used in the SHS, may yield a larger effective slip length and thus reduce the drag over the surface. This research was able to establish the foundation upon which future surfaces can be developed.

8. References

Amarouchene, Yacine, Bonn, Daniel, Kellay, Hamid, Lo, Ting-Shek, L'vov, Victor S., and Procaccia Itamar, 2008, "Reynolds Number Dependence of Drag Reduction by Rodlike Polymers," *Physics of Fluids* 20, 065108 (2008).

Brigham Young University, 2013, retrieved April 15, 2013 from http://me.byu.edu/content/research-group/Fluid%20Mechanics

Daniello, Robert J., Waterhouse, Nicholas E., and Rothstein, Jonathan P., 2009, "Drag Reduction in Turbulent Flows over Superhydrophobic Surfaces," Phys. Fluids 21, 085103 (2009).

Elbing, Bryan R. Winkel, Eric S., Lay, Keary A., Ceccio, Steven L., Dowling, David R., Perlin, Marc., 2008, "Bubble-induced skin-friction drag reduction and the abrupt transition to air-layer drag reduction." J. Fluid Mech. (2008), vol. 612, pp. 201–236.

Esmail, M.A. Mokheimer, Maged El-Shaarawi, 2005, "Maximum possible induced flow rates in open-ended vertical eccentric annuli with uniform heat flux," International Journal of Numerical Methods for Heat & Fluid Flow, Vol. 15 Iss: 2, pp.161 – 182

Flack, Karen, Schultz, Michael P. and Shapiro, Thomas. 2005 "Experimental support for Townsend's Reynolds number similarity hypothesis on rough walls." Phys. Fluids 17, 035102 (2005)

García-Mayoral, Ricardo and Jiménez, Javier, 2011, "Drag Reduction by Riblets," Phil. Trans. R. Soc. A (2011) 369, 1412–1427.

Hefner, Jerry M., 1990, "Viscous Drag Reduction in Boundary Layers," Retrieved January 15, 2012, from http://books.google.com

Kim, Philseok, 2013, "Fabrication of SLIPS on Metallic Surfaces and Preliminary Drag Characterizations," ONR MURI Review Meeting, January 25, 2013.

Kodama Y., Kakugawa, A. Takahashi, T., and Nagaya S., 2000, "Drag Reduction of Ships by Microbubbles," National Maritime Research Institute of Japan, Retrieved January 15, 2012, from http://www.nmri.go.jp/main/cooperation/ujnr/24ujnr_paper_jpn/kodama.pdf

LaVision, "Laser Doppler Velocimetry/Phase Doppler Interferometry," Retrieved January 15, 2012, from http://www.lavision.de/en/techniques/ldv_pdi.php

Lumley, J. L., 1973, "Drag Reduction in Turbulent Flow by Polymer Additives," *Journal of Polymer Science: Macromolecular Reviews* Volume 7, Issue 1, pages 263–290, 1973.

Makiharju, Simo, Lay, Keary, Yakushiji, Ryo, Perlin, Marc, and Steven Ceccio, 2008, "Lay-Language version of 'Partial Cavity Drag Reduction,'" 61st APS Division of Fluid

Dynamics Meeting (November 24, 2008), Retrieved February 27, 2012, from http://www.aps.org/units/dfd/pressroom/papers/ships.cfm

Martell, Michael B., Perot, J. Blair, and Rothstein, Jonathan P., 2009, "Direct Numerical Simulations of Turbulent Flows over Superhydrophobic Surfaces," J. Fluid Mech. (2009), vol. 620, pp. 31-41.

Martell, Michael B., Rothstein, Jonathan P., and Perot, J. Blair, 2010, "An Analysis of Superhydrophobic Turbulent Drag Reduction Mechanisms using Direct Numerical Simulation," *Physics of Fluids* 22, 065102 (2010).

McCormick, Michael E., and Bhattacharyya Rameswar, 1973, "Drag Reduction of a Submersible Hull by Electrolysis," *Naval Engineers Journal*, Volume 85, Issue 2, pages 11–16, April 1973.

Muralidhar, Pranesh, Ferrer, Nangelie, Daniello, Robert, and Jonathan P. Rothstein, 2011, "Influence of Slip on the Flow Past Superhydrophobic Circular Cylinders," J. Fluid Mech. (2011), vol. 680, pp. 459-476.

Rothstein, J.P. 2010, "Slip on Superhydrophobic Surfaces," Annual Review of Fluid Mechanics, (2010), vol. 42: 89-109.

RWTH, "Technical Flow and Sub-Processes," Retrieved January 15, 2012, from http://www.iww.rwth-aachen.de/en/menue/about_us/research/hydromechanics.html

Schetz, Joseph A. 1993. *Boundary Layer Analysis*. Prentice Hall, New Jersey.

Schultz, M. P., Bendick, J. A., Holm, E. R. and Hertel, W. M., 2011, "Economic impact of biofouling on a naval surface ship," Biofouling, 27: 1, 87 — 98, First published on: 14 December 2010 (iFirst)

Toonder, Jacob Marinus Jan den, 1995, "Drag Reduction by Polymer Additives in a Turbulent Pipe Flow: Laboratory and Numerical Experiments," Retrieved January 15, 2012 from http://www.mate.tue.nl/~hulsen/papers_open/1733.pdf

Perlin, Marc and Ceccio, Steven, 2013, "Air Layer Drag Reduction; Partial Cavity Drag Reduction," retrieved April 15, 2013 from http://name.engin.umich.edu/marine-hydrodynamics-laboratory/specialty-tests/air-layer-drag-reduction-partial-cavity-drag-reduction